































# PITX2 deficiency leads to atrial mitochondrial dysfunction

Jasmeet S. Reyat <sup>1,2,\*§</sup>, Laura C. Sommerfeld <sup>1,3,4,5§</sup>, Molly O'Reilly <sup>1</sup>, Victor Roth Cardoso <sup>1,6</sup>, Ellen Thiemann <sup>3,4,7</sup>, Abdullah O. Khan <sup>1</sup>, Christopher O'Shea <sup>1</sup>, Sönke Harder <sup>8</sup>, Christian Müller<sup>9</sup>, Jonathan Barlow <sup>10</sup>, Rachel J. Stapley <sup>1</sup>, Winnie Chua <sup>1</sup>, S. Nashitha Kabir <sup>1</sup>, Olivia Grech <sup>1</sup>, Oliver Hummel <sup>11</sup>, Norbert Hübner <sup>11,12,13</sup>, Stefan Käb <sup>14,15</sup>, Lluís Mont <sup>16,17,18</sup>, Stéphane N. Hatem<sup>19</sup>, Joris Winters <sup>20</sup>, Stef Zeemering <sup>20</sup>, Neil V. Morgan <sup>1</sup>, Julie Rayes <sup>1</sup>, Katja Gehmlich <sup>1</sup>, Monika Stoll <sup>21,22</sup>, Theresa Brand <sup>23</sup>, Michaela Schweizer <sup>24</sup>, Angelika Piasecki<sup>7</sup>, Ulrich Schotten <sup>20</sup>, Georgios V. Gkoutos <sup>6</sup>, Kristina Lorenz <sup>23,25</sup>, Friederike Cuello <sup>4,7</sup>, Paulus Kirchhof <sup>1,3,4,\*</sup>, and Larissa Fabritz <sup>1,3,4,5</sup>

<sup>1</sup>Institute of Cardiovascular Sciences, College of Medical and Dental Sciences, University of Birmingham, Wolfson Drive, B15 2TT Birmingham, UK; <sup>2</sup>Division of Cardiovascular Medicine, Radcliffe Department of Medicine, University of Oxford, John Radcliffe Hospital, OX3 9DU Oxford, UK; <sup>3</sup>Department of Cardiology, University Heart and Vascular Center Hamburg, University Medical Center Hamburg-Eppendorf, Martinistraße 52, 20246 Hamburg, Germany; <sup>4</sup>DZHK (German Center for Cardiovascular Research), Partner Site Hamburg/Kiel/Lübeck, University Medical Center Hamburg-Eppendorf, Martinistraße 52, 20246 Hamburg, Germany; <sup>5</sup>University Center of Cardiovascular Sciences, University Medical Center Hamburg-Eppendorf, Martinistraße 52, 20246 Hamburg, Germany; <sup>6</sup>Institute of Cancer Genomics, College of Medical and Dental Sciences, University of Birmingham, B15 2TT Birmingham, UK; <sup>7</sup>Institute of Experimental Pharmacology and Toxicology, Cardiovascular Research Center, University Medical Center Hamburg-Eppendorf, Martinistrasse 52, 20246 Hamburg, Germany; <sup>8</sup>Institut für Klinische Chemie und Laboratoriumsmedizin, Massenspektrometrische Proteomanalytik, University Medical Center Hamburg-Eppendorf, Martinistrasse 52, 20246 Hamburg, Germany; <sup>9</sup>UKE Bioinformatics Core, University Medical Center Hamburg-Eppendorf, Martinistrasse 52, 20246 Hamburg, Germany; <sup>10</sup>Cellular Health and Metabolism Facility, College of Life and Environmental Sciences, University of Birmingham, B15 2TT Birmingham, UK; <sup>11</sup>Max Delbrück Centrum for Molecular Medicine, Robert-Rössle-Straße 10, 13125 Berlin, Germany; <sup>12</sup>Charité—Universitätsmedizin Berlin, Charitéplatz 1, 10117 Berlin, Germany; <sup>13</sup>DZHK (German Center for Cardiovascular Research), Partner Site Berlin, Germany; <sup>14</sup>Department of Medicine I, University Hospital Munich, Ludwig Maximilian University of Munich (LMU), Marchioninistraße 15, 81377 Munich, Germany; <sup>15</sup>DZHK (German Centre for Cardiovascular Research), Partner Site Munich Heart Alliance, Munich, Germany; <sup>16</sup>Hospital Clínic, Universitat de Barcelona, Villarroel, 170, 08036, Barcelona, Catalonia, Spain; <sup>17</sup>Institut de Recerca Biomèdica, August Pi i Sunyer, Roselló, 149-153, 08036 Barcelona, Catalonia, Spain; <sup>18</sup>Centro Investigación Biomédica en Red Cardiovascular, Av. Monforte de Lemos, 3-5. Pabellón 11. Planta 0, 28029 Madrid, Spain; <sup>19</sup>INSERM UMR5116, ICAN—Institute of Cardiomatobiology and Nutrition, Sorbonne University, Institut de Cardiologie, Pitié-Salpêtrière Hospital, 91 Boulevard de l'Hôpital, 75013 Paris, France; <sup>20</sup>Department of Physiology, Cardiovascular Research Institute Maastricht, Maastricht University, Minderbroedersberg 4-66211 LK Maastricht, The Netherlands; <sup>21</sup>Institute of Human Genetics, Genetic Epidemiology, WWU Münster, Albert-Schweitzer-Campus 1, D3, Domagkstraße 3, 48149 Münster, Germany; <sup>22</sup>Cardiovascular Research Institute Maastricht, Genetic Epidemiology and Statistical Genetics, Maastricht University, Universiteitssingel 50, 6229 ER Maastricht, The Netherlands; <sup>23</sup>Institute of Pharmacology and Toxicology, University of Würzburg, Versbacher Straße 9, 97078 Würzburg, Germany; <sup>24</sup>Department of Morphology and Electron Microscopy, Center for Molecular Neurobiology, University Medical Center Hamburg-Eppendorf, Martinistraße 52, 20246 Hamburg, Germany; and <sup>25</sup>Leibniz-Institut für Analytische Wissenschaften—ISAS—e.V., ISAS City, Bunsen-Kirchhoff-Straße 11, 44139 Dortmund, Germany

Received 1 September 2023; revised 27 April 2024; accepted 23 May 2024; online publish-ahead-of-print 12 August 2024

**Time of primary review: 30 days**

## Aims

Reduced left atrial *PITX2* is associated with atrial cardiomyopathy and atrial fibrillation (AF). *PITX2* is restricted to left atrial cardiomyocytes (aCMs) in the adult heart. The links between *PITX2* deficiency, atrial cardiomyopathy, and AF are not fully understood.

## Methods and results

To identify mechanisms linking *PITX2* deficiency to AF, we generated and characterized *PITX2*-deficient human aCMs derived from human induced pluripotent stem cells (hiPSC) and their controls. *PITX2*-deficient hiPSC-derived atrial cardiomyocytes showed shorter and disorganized sarcomeres and increased mononucleation. Electron microscopy found an increased number of smaller mitochondria compared with isogenic controls. Mitochondrial protein expression was altered in *PITX2*-deficient hiPSC-derived atrial cardiomyocytes. Single-nuclear RNA-sequencing found differences in cellular respiration

\* Corresponding authors. Tel: +49 40 741053824; Email: [p.kirchhof@uke.de](mailto:p.kirchhof@uke.de); Tel: +44 (0)186 523 4915; Email: [jasmeet.reyat@cardiov.ox.ac.uk](mailto:jasmeet.reyat@cardiov.ox.ac.uk)

§ The first two authors contributed equally to the study.

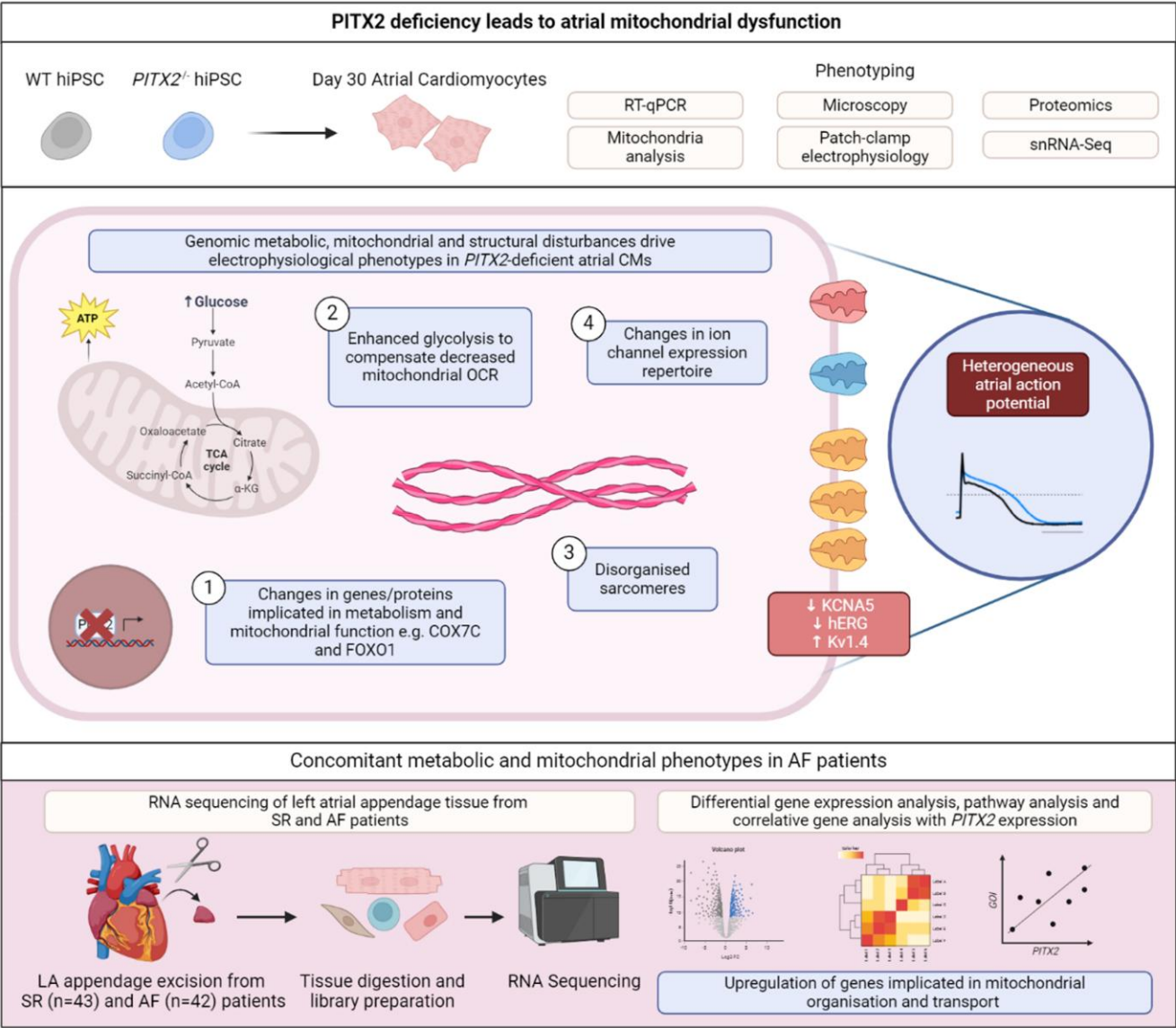
© The Author(s) 2024. Published by Oxford University Press on behalf of the European Society of Cardiology.

This is an Open Access article distributed under the terms of the Creative Commons Attribution-NonCommercial License (<https://creativecommons.org/licenses/by-nc/4.0/>), which permits non-commercial re-use, distribution, and reproduction in any medium, provided the original work is properly cited. For commercial re-use, please contact [reprints@oup.com](mailto:reprints@oup.com) for reprints and translation rights for reprints. All other permissions can be obtained through our RightsLink service via the Permissions link on the article page on our site—for further information please contact [journals.permissions@oup.com](mailto:journals.permissions@oup.com).

pathways and differentially expressed mitochondrial and ion channel genes in *PITX2*-deficient hiPSC-derived atrial cardiomyocytes. *PITX2* repression in hiPSC-derived atrial cardiomyocytes replicated dysregulation of cellular respiration. Mitochondrial respiration was shifted to increased glycolysis in *PITX2*-deficient hiPSC-derived atrial cardiomyocytes. *PITX2*-deficient human hiPSC-derived atrial cardiomyocytes showed higher spontaneous beating rates. Action potential duration was more variable with an overall prolongation of early repolarization, consistent with metabolic defects. Gene expression analyses confirmed changes in mitochondrial genes in left atria from 42 patients with AF compared with 43 patients with sinus rhythm. Dysregulation of left atrial mitochondrial (*COX7C*) and metabolic (*FOXO1*) genes was associated with *PITX2* expression in human left atria.

**Conclusion** *PITX2* deficiency causes atrial mitochondrial dysfunction and a metabolic shift to glycolysis in human aCMs. *PITX2*-dependent metabolic changes can contribute to the structural and functional defects found in *PITX2*-deficient atria.

Graphical Abstract



Deficiency in *PITX2*, a gene with left atrial and skeletal muscle expression in adults leads to mitochondrial dysfunction. *PITX2* deficiency is likely to underlie the genomic basis for atrial fibrillation (AF). Reduced *PITX2* in atrial cardiomyocytes (aCMs) conveys electrical changes and structural alterations. The cellular mechanisms linking *PITX2* deficiency to AF are not fully understood. *PITX2* deficiency increases cellular and functional heterogeneity in human iPSC-derived aCMs. These experiments show that *PITX2* alters mitochondrial function and metabolism by altering gene and protein expression in aCMs, creating a metabolic shift away from respiration towards glycolysis. Left atrial tissue from patients with AF shows similar changes in gene expression patterns of mitochondrial genes and their association with *PITX2*. Figure was generated using BioRender.com.

**Keywords**Atrial fibrillation • Mitochondrial dysfunction • Human induced pluripotent stem cells • Metabolic shift • *PITX2* • Human heart tissue

## 1. Introduction

Atrial fibrillation (AF) is common and the associated cardiovascular mortality and morbidity profoundly affect patients, their families, and society.<sup>1,2</sup> Better concepts to prevent and treat AF are needed to improve this situation.<sup>3,4</sup> Genome-wide association studies found over 100 different common gene variants that are associated with AF.<sup>5–8</sup> The most prominent signals are clustered in a genomic region on chromosome 4q25, close to the *PITX2* gene.<sup>5–8</sup> The gene variant-carrying locus regulates the *PITX2* gene,<sup>9–11</sup> and deletion of AF risk alleles reduces left atrial *PITX2* concentrations.<sup>9,10</sup> *PITX2* messenger RNA (mRNA) is confined to left atrial cardiomyocytes (aCMs) in the adult human heart<sup>12,13</sup> and in mice.<sup>12,14</sup> Recurrent AF after thoracoscopic AF ablation is related to reduced left aCM *PITX2*.<sup>13</sup> *Pitx2* mRNA regulates transcription in the adult heart<sup>15</sup> with multiple effects on cardiac function and structure: Partial deletion of *Pitx2* modulates atrial electrical function,<sup>12,16–19</sup> while complete *Pitx2* deficiency alters atrial structure, calcium handling, and ion channel composition.<sup>20–22</sup> To identify *PITX2*-dependent cellular processes and pathways contributing to these atrial changes in human cells and in patients with AF, we generated and characterized human induced pluripotent stem cell (hiPSC)-derived *PITX2*-deficient aCMs and wild-type (WT) controls. Results were validated in human left atrial tissue from patients with and without AF and compared with published findings.

## 2. Methods

### 2.1 Cell culture

Based on the known effects of *PITX2* deletion in murine and zebrafish models, we chose to delete the intron-exon region of exon 6 of the *PITX2* gene for this study to enable observation of a clear *PITX2*-dependent phenotype.<sup>19–22</sup> The human control iPSC line (F1; MPIMB011-A) and the otherwise isogenic, genome-edited *PITX2*-deficient line were donated by the group of Boris Greber and have previously been described.<sup>23</sup> HiPSCs were maintained in Gibco StemFlex Medium (Thermo Fisher Scientific, Rugby, A3349401) on Geltrex (Thermo Fisher Scientific, A1569601)-coated plates. The differentiation of hiPSCs into atrial cardiomyocytes and ventricular cardiomyocytes (vCMs) was optimized based on a published protocol.<sup>24</sup> Briefly, on day 0, the medium was replaced with differentiation medium [RPMI-1640 with GlutaMAX<sup>TM</sup> and HEPES (Thermo Fisher Scientific, 72400047) containing 0.5 mg/mL human recombinant albumin (Sigma-Aldrich, Gillingham, A9731), 0.2 mg/mL L-ascorbic acid 2-phosphate (Sigma-Aldrich, 49752)] supplemented with 4  $\mu$ M CHIR99021 (Sigma-Aldrich, SML1046) to promote mesoderm induction. On day 2, the medium was replaced with a differentiation medium containing 5  $\mu$ M IWP-2 (Sigma-Aldrich, I0536) to promote cardiac progenitor cell differentiation. After day 4, cells were maintained in the cardiomyocyte differentiation medium. To induce aCM specification, 1  $\mu$ M retinoic acid (Sigma-Aldrich, R2625) was supplemented to the medium between days 3 and 6 of differentiation. On day 6, the medium was changed to cardiomyocyte maintenance medium [cardiomyocyte differentiation medium supplemented with 2% B-27<sup>TM</sup>, Thermo Fisher Scientific, 17504044], and the medium was refreshed every 48 h. Beating cardiomyocytes were observed from as early as day 8 of differentiation. At day 12, aCMs and vCMs were re-plated at a lower density by dissociating cells using StemPro Accutase Cell Dissociation Reagent (Thermo Fisher Scientific, A1110501) and cultured in cardiomyocyte plating medium [cardiomyocyte maintenance

medium with the addition of 10% KnockOut<sup>TM</sup> Serum (Gibco, 10828028) and 1  $\mu$ M Thiazovivin (Sigma-Aldrich, SML1045)] for 24 h before the medium was changed to cardiomyocyte selection medium [RPMI 1640 no glucose (Gibco, 11879020) supplemented with 0.5 mg/mL human recombinant albumin, 0.2 mg/mL L-ascorbic 2-phosphate and 4 mM lactate (Sigma-Aldrich, 1614308)] for an additional five days. Afterwards, aCMs and vCMs were maintained in a cardiomyocyte maintenance medium until day 30, a time-point in which hiPSC-derived aCMs and vCMs express key cardiac markers.<sup>24,25</sup>

### 2.2 Immunofluorescence staining

HiPSC-derived atrial cardiomyocytes were fixed with 4% paraformaldehyde, blocked with 4% goat serum, and incubated with primary antibodies (see [Supplementary material online, Table S1](#)) overnight at 4°C on a rocker. Cells were subsequently washed and stained with the corresponding Alexa Fluor secondary antibody conjugates (Thermo Fisher Scientific) for 1 h at room temperature and then counterstained with DAPI (1:10,000) for 5 min and mounted using Prolong Gold Anti-fade reagent (Thermo Fisher Scientific) ready for imaging using a Zeiss LSM 880 Airyscan confocal microscope (Carl Zeiss NTS Ltd., Oberkochen). Images were analysed using Fiji software. Sarcomere structure analysis was carried out using a previously published MATLAB (MathWorks) script.<sup>26</sup> Analysis of nuclei parameters was carried out using a previously described pipeline in Cell Profiler 4.2.1.<sup>27</sup>

### 2.3 Electron microscopy

HiPSC-derived atrial cardiomyocytes were cultured in 3.5-cm plastic dishes for 3 days, fixed in a mixture of 4% paraformaldehyde and 1% glutaraldehyde (Science Services, ) in 0.1 M phosphate buffer overnight at 4°C. Samples were rinsed three times in 0.1 M sodium cacodylate buffer (pH 7.2–7.4), scraped off the cell culture dish, and osmicated using 1% osmium tetroxide in cacodylate buffer. Following osmication, the samples were dehydrated using ascending ethanol concentrations, followed by two rinses in propylene oxide. Infiltration of the embedding medium was performed by immersion in a 1:1 mixture of propylene oxide and Epon (Science Services, Germany), followed by neat Epon and hardening at 60°C for 48 h. For electron microscopy, ultra-thin sections (60 nm) were cut and mounted on copper grids and stained using uranyl acetate and lead citrate. The sections were analysed with a JEM- 2100Plus Transmission Electron Microscope at 200 kV (Jeol, Germany). Images were acquired with the XAROSA CMOS camera (Emsis, Germany).

### 2.4 Flow cytometry

HiPSC-derived atrial cardiomyocytes were processed using the FoxP3/Transcription Factor Staining Buffer kit (eBiosciences<sup>TM</sup>, 00–5523–00) according to manufacturer's instructions before being incubated with primary antibodies (see [Supplementary material online, Table S1](#)) overnight at 4°C on a rocker. Subsequently, samples were induced with corresponding Alexa Fluor secondary antibody conjugates (Thermo Fisher Scientific) for 30 min at 4°C. For experiments looking at cell proliferation, hiPSC-derived atrial cardiomyocytes were incubated with 5-ethynyl-2'-deoxyuridine (EDU) using the Click-iT<sup>TM</sup> EDU Alexa Fluor 488 Flow Cytometry Assay Kit (Thermo Fisher Scientific, C10420) according to the manufacturer's instructions. Samples were processed using a BD LSR Fortessa<sup>TM</sup> (BD Biosciences), and data were analysed using FlowJo software.

## 2.5 RNA isolation and quantitative real-time PCR

Total RNA was isolated from aCMs and vCMs using the RNeasy Mini Kit (QIAGEN, 74104) and reverse transcribed into cDNA using the High-Capacity cDNA Reverse Transcription Kit (Applied Biosystems, 4368814) using a total of 1 µg of RNA. RNA was quantified using the Qubit<sup>TM</sup> RNA high-sensitivity kit (Invitrogen, Q32852) using a Qubit Fluorometer. cDNA was diluted to a working concentration of 5 ng/µL using RNA-free water (QIAGEN, 129112). Quantitative real-time PCR (RT-qPCR) was performed using 10 ng of template cDNA and PowerUp<sup>TM</sup> SYBR<sup>TM</sup> Green Master Mix (Applied Biosystems, A25742). Samples were run on the 7500 Fast Real-Time PCR system (Thermo Fisher Scientific). Gene of interest Ct values were normalized to housekeeping gene Ct values using the  $\Delta\Delta Ct$  method.<sup>28</sup> Sequences of primers used for RT-qPCR are provided in [Supplementary material online, Table S2](#).

## 2.6 Proteomics

Protein quantification, quality assessment, imputation, differential expression analysis, and enrichment analyses were conducted by the UKE Bioinformatics Core, Hamburg, Germany. hiPSC-derived atrial cardiomyocytes from six independent differentiation runs were pelleted, washed with sterile PBS, and shock-frozen in liquid nitrogen. Samples were prepared using established proteomic techniques (for details see [Supplementary materials and methods](#)).

## 2.7 Extracellular flux analysis

Mitochondrial oxidative phosphorylation and glycolytic flux were measured with a Seahorse XF-96 Analyser (Agilent). hiPSC-derived atrial cardiomyocytes were plated into XF-96 well (Agilent, 103794-100) Geltrex-coated plates at a cell density of 50 000 cells per well. Measurements were made in XF RPMI Medium pH 7.4 supplemented with 10 mM glucose, 1 mM HEPES, 2 mM L-Glutamine, and 1 mM sodium pyruvate. Mitochondrial oxidative phosphorylation and glycolytic proton efflux were assessed using the following parameters: oligomycin (2 µg/mL), BAM15 (3 µM), rotenone and antimycin A (2 µM), and desoxyglucose (2-DG; 50 mM). ATP supply fluxes and corrections of mitochondrial acidification were calculated as previously described.<sup>29–31</sup>

## 2.8 Analysis of mitochondrial membrane potential

The mitochondrial membrane potential was analysed using the mitochondrial-selective dye tetramethylrhodamine methyl ester (TMRM; 2.5 nM). To normalize mitochondrial content, hiPSC-derived atrial cardiomyocytes were stained with MitoTrackerGreen (200 nM, 1 h). hiPSC-derived atrial cardiomyocytes were plated on gelatine-coated glass coverslips and cultured for 6–7 days at 5% CO<sub>2</sub> and 37°C. Measurements were performed on a Leica TCS SP5 confocal microscope at basal conditions or in response to oligomycin A treatment (2 µM). TMRM was excited at 561 nm and emission assessed between 580 and 700 nm. MitoTrackerGreen was excited at 488 nm and emission assessed between 500 and 530 nm. The images were processed using LAS X software (version 3.5.6.21594). Mean intensity values of TMRM fluorescence (corrected for background) were normalized to the mean intensity value of MitoTrackerGreen fluorescence (corrected for background) per image to correct for mitochondrial content.  $n = 3$  independent hiPSC-derived atrial cardiomyocyte differentiation runs and 20 images per condition per hiPSC-derived atrial cardiomyocyte batch were analysed. Data were normalized to mean values of WT hiPSC-derived atrial cardiomyocytes at basal conditions.

## 2.9 Western blotting

Protein isolation and western blotting were carried out as previously described.<sup>13</sup> Briefly, proteins were isolated from hiPSC-derived atrial cardiomyocytes using 1% Triton X-100 (Sigma-Aldrich, T8787) and protease and phosphatase inhibitors (Thermo Fisher, 78440) and subsequently

quantified using the DC Protein Assay kit (Bio-Rad, 500-01112). SDS-polyacrylamide gel electrophoresis and western blot analysis were performed using Novex<sup>TM</sup> WedgeWell<sup>TM</sup> 4–20% Tris-Glycine gels (Thermo Fisher, XP04205). Membranes were blocked in Intercept® (Tris-buffered Saline) blocking buffer (LI-COR, 927-60001) and incubated at 4°C overnight on an orbital shaker. On the next day, membranes were incubated overnight at 4°C with primary antibodies (see [Supplementary material online, Table S1](#)). Membranes were then washed and incubated with mouse and rabbit fluorescently conjugated secondary antibodies (LI-COR) for 2 h at room temperature before visualization on the LI-COR Fc Dual-Mode Imaging System. Quantification of western blots was carried out using Image Studio Lite software (LI-COR) with quantification normalized to GAPDH expression.

## 2.10 Single-nuclei RNA-sequencing of WT and *PITX2*<sup>-/-</sup> hiPSC-derived atrial cardiomyocytes and analysis

In order to assess changes in gene expression resulting from suppression of the *PITX2* gene at the single-cell level, we applied single-nuclei RNA-sequencing (snRNAseq) to hiPSC-derived atrial cardiomyocytes. Nuclei from hiPSC-derived atrial cardiomyocytes were isolated and processed for snRNAseq as described.<sup>32</sup> We compared two replicates of the *PITX2*<sup>-/-</sup> hiPSC-derived atrial cardiomyocyte cell line with three replicates of the WT hiPSC-derived atrial cardiomyocytes as controls. Data were mapped to the human genome (GRCh38) using 10X cellranger version 6.1.2 ([www.10xgenomics.com](http://www.10xgenomics.com)), processed to remove doublets and identify nuclei that met high-quality standards, and harmonized to remove batch effects.<sup>33</sup> Manifolds were constructed using Uniform Manifold Approximation and Projections (UMAPs) for all individual nuclei of knock-out and control samples (<https://arxiv.org/pdf/1802.03426.pdf>). Populations were defined by assignment of nuclei to individual clusters based on Leiden-annotation with a resolution of 0.5.<sup>34</sup> To perform differential gene expression analyses (DGE) between *PITX2*<sup>-/-</sup> hiPSC-derived atrial cardiomyocytes and WT groups we created aggregated pseudo-bulk samples from our single-nuclei dataset (one pseudo-bulk sample per each cluster/Leiden annotated<sup>35</sup>). To be considered, one sample should have at least five nuclei per cluster. To test for DGE we used edgeR implemented in R. Before fitting our quasi-likelihood negative binomial generalized log-linear model, we filtered for genes that have sufficient counts (at least 10) and that were expressed in at least 50% of the samples ( $\text{min.prop} = 0.5$ ) to be considered in statistical analysis. We used the empirical Bayes quasi-likelihood test (`glmQLFtest`) to perform gene-wise tests across contrasts. Pathway enrichment analysis of RNAseq data from aCM was performed using Bioconductor packages in R (Version 4.3.3) and RStudio (Version 2023.12.1). To compare gene expression changes in response to *PITX2* repression, a recently published data set of hiPSC-derived ventricular-like cardiomyocytes exposed to *PITX2*-repressing siRNA or to scrambled control RNA was accessed.<sup>36</sup> Pathway analysis using gene ontology and expression of metabolic differentially expressed genes of interest was performed. Kyoto Encyclopedia of Genes and Genomes pathways and GO terms of differentially expressed genes were determined by Benjamini–Hochberg tests with a *P*-value threshold of 0.05.

## 2.11 Whole-cell patch-clamp electrophysiology

hiPSC-derived atrial cardiomyocytes were plated at a density of 25 000–35 000 cells on Geltrex-coated 15 mm round glass coverslips to obtain single-cell distribution. The cells were maintained in culture for a minimum of seven days until experiments were carried out. Action potential (AP) recordings were made using the whole-cell patch-clamp technique on an Axopatch 200B amplifier (Molecular Devices), recorded in the current-clamp configuration. Briefly, cells were superfused at 3 mL/min, 36–37°C, with a solution containing in mM: 145 NaCl, 5.4 KCl, 5 HEPES, 1.8 CaCl<sub>2</sub>, 1.2 MgCl<sub>2</sub>, 0.33



NaH<sub>2</sub>PO<sub>4</sub>, 0.83 MgSO<sub>4</sub>·7H<sub>2</sub>O, and 11 glucose, pH 7.4 with NaOH. The internal pipette solution contained in mM: 130K-glutamate, 10 KCl, 10 NaCl, 0.5 MgCl<sub>2</sub>, 10 HEPES, and 5 MgATP, pH 7.2 with KOH (all reagents from Sigma-Aldrich). Pipette resistance ranged between 1.5 and 3 MΩ. Spontaneously occurring APs were recorded for 60 s before APs were triggered by 1 ms current injections (1 nA). AP trains were stimulated at 1, 2, or 3 Hz for 60 s to allow rate adaptation and digitized at 50 kHz using CED micro1401 driven by Signal v6 (Cambridge Electronic Design). Only spontaneously beating cells were used for experiments. APs were analysed for diastolic membrane potential and AP duration (APD30, APD50, APD70, and APD90) using modified algorithms from ElectroMap software.<sup>37</sup> Information on additional parameters measured can be found in the [Supplementary materials](#) online.

## 2.12 Bulk RNA-sequencing of human left atrial appendages and analysis

Bulk RNA-sequencing was performed on human left atrial appendages (see study approval) collected from patients undergoing open-heart surgery with excision of left and right atria at six centres as published.<sup>13</sup> Sequencing was performed at the University of Münster, Germany (M Stoll). Good-quality samples were aligned to the human genome (GRCh38p12) using the HISAT2 alignment tool.<sup>38</sup> The aligned files were sorted and indexed using samtools.<sup>39</sup> Feature counts (transcript level) were computed using the htseq tool.<sup>38</sup> Htseq readcounts were normalized using DESeq2. Data was transformed using regularized log transformation with DESeq2 prior to visualization. DGE analysis was performed by modelling the Benjamini–Hochberg false discovery rate (FDR). Differentially expressed genes were defined as FDR <0.05 and Log<sub>2</sub>(fold change) >0.1. For heatmaps, data were visualized as log-normalized counts from DESeq2. GO Pathway Enrichment analysis was carried out using Gene Ontology.

## 2.13 Statistical analysis

Data were analysed using PRISM (GraphPad Software Inc., version 6), and results are presented as mean ± SD unless otherwise stated. All experiments were repeated a minimum of three times using different batches of differentiated cells accounting for biological replicates, which are specified in the figure legends. The number of samples (*n*) and the statistical test used for each analysis are indicated in the figure legends. Where possible, experimenters were blinded to the genotypes of tissue samples/cells. *P*-values are stated in the figures.

## 2.14 Study approval

Biopsies from left atrial appendages were sampled during open-heart surgery from six separate cohort studies run at the universities of Barcelona, Birmingham, Maastricht, Muenster, Munich, and Paris (all part of the CATCH ME consortium), and immediately frozen in liquid nitrogen to prevent RNA degradation. All study participants provided written informed consent. The investigation complied with the principles that govern the use of human tissues outlined in the Declaration of Helsinki. The Medical Ethics Committee of each participating centre approved the study and its protocols. Overall governance was provided by Maastricht University. Details of the clinical characteristics of the patients have been published.<sup>40</sup> This analysis compared patients who were in sinus rhythm (SR) at the time of surgery and who did not have a history of AF prior to surgery (SR) with patients who had established, permanent AF.

# 3. Results

## 3.1 Generation and differentiation of PITX2-deficient hiPSC-derived atrial cardiomyocytes

PITX2-deficient hiPSC line and the respective control (WT) cells showed a normal karyotype and pluripotency status (see [Supplementary material](#)

[online, Figure S1A–C](#)). PITX2-deficient hiPSCs and WT hiPSCs were successfully differentiated into aCMs ([Figure 1A](#)) with a high yield (see [Supplementary material online, Figure S1D](#)). Time course analysis revealed robust induction of PITX2 expression, peaking between days 8 and 12 of differentiation in WT cells ([Figure 1B](#)). This early peak reflects the known role of PITX2 in right-left patterning during early mesodermal development.<sup>41–43</sup> BMP10 expression was detected from 30 days of differentiation, reflecting differentiation of the cells into hiPSC-derived atrial cardiomyocytes ([Figure 1C](#)).<sup>24,25</sup> As intended, PITX2 was reduced in PITX2<sup>−/−</sup> hiPSC-derived atrial cardiomyocytes ([Figure 1D](#)). As expected, WT hiPSC-derived vCMs showed no PITX2 expression ([Figure 1D](#)). Subsequent analysis of cardiomyocyte developmental transcriptional factors revealed a reduction in MYCOD and an increase in TBX5 expression in the PITX2<sup>−/−</sup> hiPSC-derived atrial cardiomyocytes (see [Supplementary material online, Figure S2A](#)). aCM markers BMP10, KCNJ3, NR2F1, and NR2F2 expression was reduced as expected (see [Supplementary material online, Figure S2B](#)). Ventricular-specific genes were largely undetectable in WT and PITX2<sup>−/−</sup> hiPSC-derived atrial cardiomyocytes (see [Supplementary material online, Figure S2C](#)).

## 3.2 Altered cardiomyocyte structure and nuclear morphology in PITX2-deficient hiPSC-derived atrial cardiomyocytes

PITX2<sup>−/−</sup> hiPSC-derived atrial cardiomyocytes exhibited sarcomere disarray ([Figure 1E](#)) and shortened sarcomeres ([Figure 1F](#)) compared with WT controls. mRNA concentrations of the sarcomeric transcripts MYH6, TNNT2, and TNNI1 mRNA were increased in PITX2<sup>−/−</sup> hiPSC-derived atrial cardiomyocytes compared with WT controls ([Figure 1G](#)). PITX2<sup>−/−</sup> hiPSC-derived atrial cardiomyocytes displayed a greater ratio of mono-nucleated cardiomyocytes compared with multi-nucleated cardiomyocytes ([Figure 1H](#)). These nuclei were increased in number, larger, and displayed an altered shape (see [Supplementary material online, Table S4](#)). Given that mononucleation is associated with an increased proliferative capacity in cardiomyocytes,<sup>44</sup> we next investigated the proliferation status of PITX2<sup>−/−</sup> hiPSC-derived atrial cardiomyocytes. PITX2<sup>−/−</sup> hiPSC-derived atrial cardiomyocytes displayed increased 5-ethynyl-2'-deoxyuridine (EdU) incorporation compared with WT hiPSC-derived atrial cardiomyocytes (see [Supplementary material online, Figure S2D](#)) and showed a proliferative gene signature with increased expression of CCNA1 and CCNB1 (see [Supplementary material online, Figure S2E](#)) and a reduction in the cellular quiescence genes TP53, CDKN1a, CDKN2a and HES1 (see [Supplementary material online, Figure S2F](#)), confirming increased proliferation.

## 3.3 Proteomic analysis identifies altered mitochondrial and metabolic pathways in PITX2-deficient hiPSC-derived atrial cardiomyocytes

Principal component analysis of the proteomic data revealed close clustering of the PITX2<sup>−/−</sup> hiPSC-derived atrial cardiomyocytes ([Figure 2A](#)). In total, 150 out of 3128 proteins were differentially expressed between genotypes ([Figure 2B](#)). Gene-Set Enrichment Analysis identified differentially expressed mitochondrial proteins ([Figure 2C](#)) and up-regulated Normalized Enrichment Scores in PITX2<sup>−/−</sup> hiPSC-derived atrial cardiomyocytes for processes affecting mitochondria, the generation of metabolites, energy allocation and mitochondrial translation and organization, specifically of the cristae and enhanced collagen biosynthesis ([Figure 2D](#)). Endoplasmic reticulum and ribosome organization, translation, and extracellular matrix organization were down-regulated. These data identify a link between PITX2 deficiency and expression of proteins relevant to mitochondrial and metabolic function in hiPSC-derived atrial cardiomyocytes. Targeted comparisons of key proteins relevant for mitochondrial fission and fusion ([Figure 2E](#)) and of mitophagy and biogenesis ([Figure 2F](#)) were differentially expressed in PITX2<sup>−/−</sup> hiPSC-derived atrial cardiomyocytes.

PITX2-dependent changes in gene expression based on single-nuclear RNA-sequencing pseudo-bulk analysis of single-nuclei RNA-sequencing

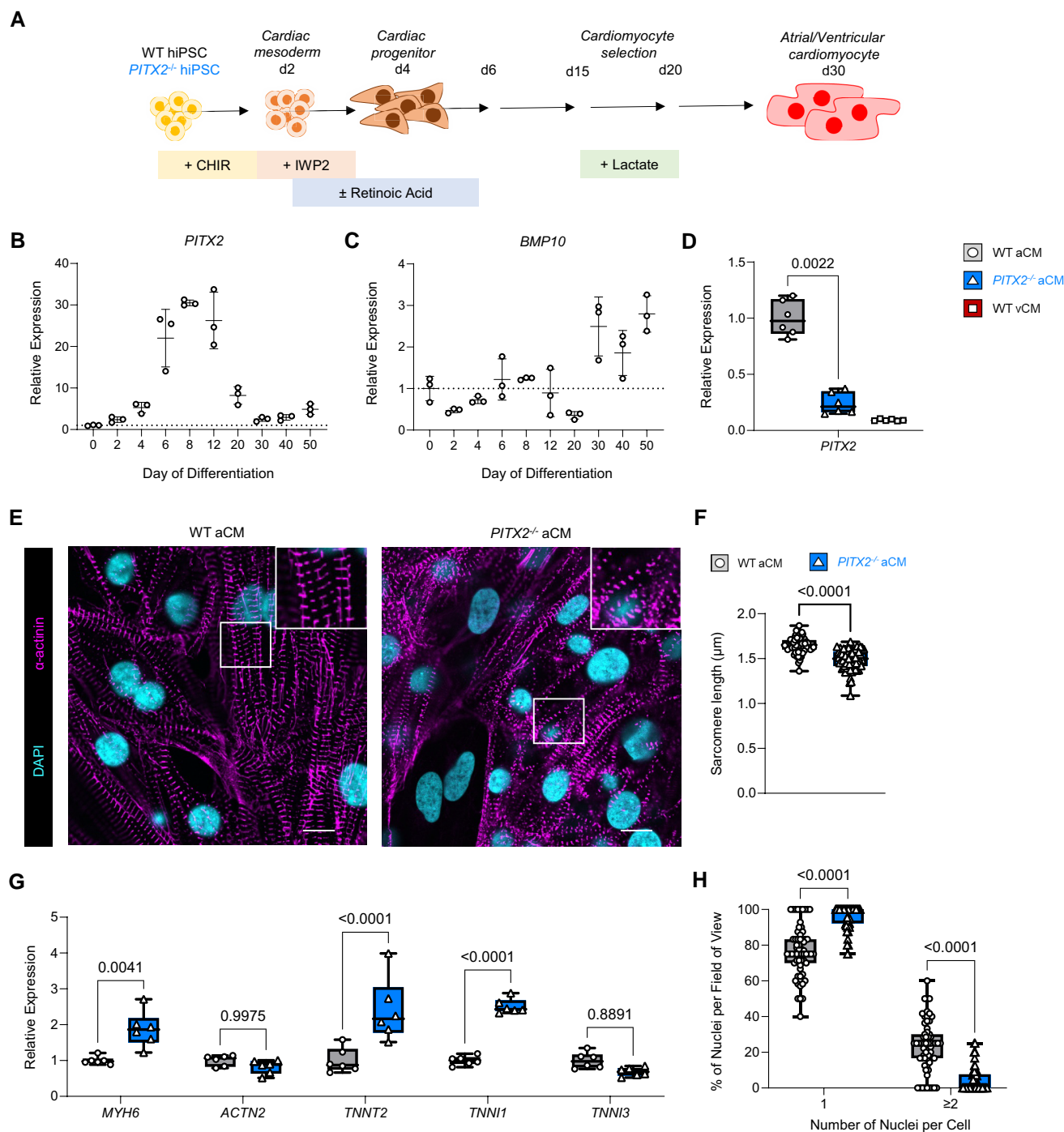


**Figure 1** Characterization of WT and  $PITX2^{-/-}$  hiPSC-derived atrial cardiomyocytes (aCMs). (A) Schematic overview of differentiation protocol used to generate hiPSC-derived aCMs. (B) Gene expression analysis of *PITX2* and (C) *BMP10* over the time course of atrial cardiomyocyte differentiation using WT hiPSC-derived aCMs (WT aCMs) as assessed by RT-qPCR ( $n = 3$ ). Dashed line represents the basal expression of *PITX2* or *BMP10* in WT hiPSCs. (D) Gene expression of *PITX2* in day 30 aCMs from WT and  $PITX2^{-/-}$  ( $PITX2^{-/-}$  aCMs) lines as assessed by RT-qPCR. Day 30 hiPSC-derived ventricular cardiomyocytes from the WT line (WT vCMs) were used as a control ( $n = 6$ ). (E) Confocal microscopy of immunofluorescently labelled  $\alpha$ -actinin in WT and  $PITX2^{-/-}$  aCMs. Scale bar = 10  $\mu$ m. (F) Sarcomere length measurements in WT and  $PITX2^{-/-}$  aCMs (WT aCMs = 63 images;  $PITX2^{-/-}$  aCMs = 62 images). (G) Gene expression of *MYH6*, *ACTN2*, *TNNT2*, *TNNI1* and *TNNI3* in WT and  $PITX2^{-/-}$  aCMs as assessed by RT-qPCR ( $n = 6$ ). Data are expressed as the mean relative expression and presented as box and whisker plots (min to max). Mann-Whitney  $U$  tests were used to compare gene concentrations between groups. (H) Bi-nucleated and mono-nucleated cell analysis in WT and  $PITX2^{-/-}$  aCMs.

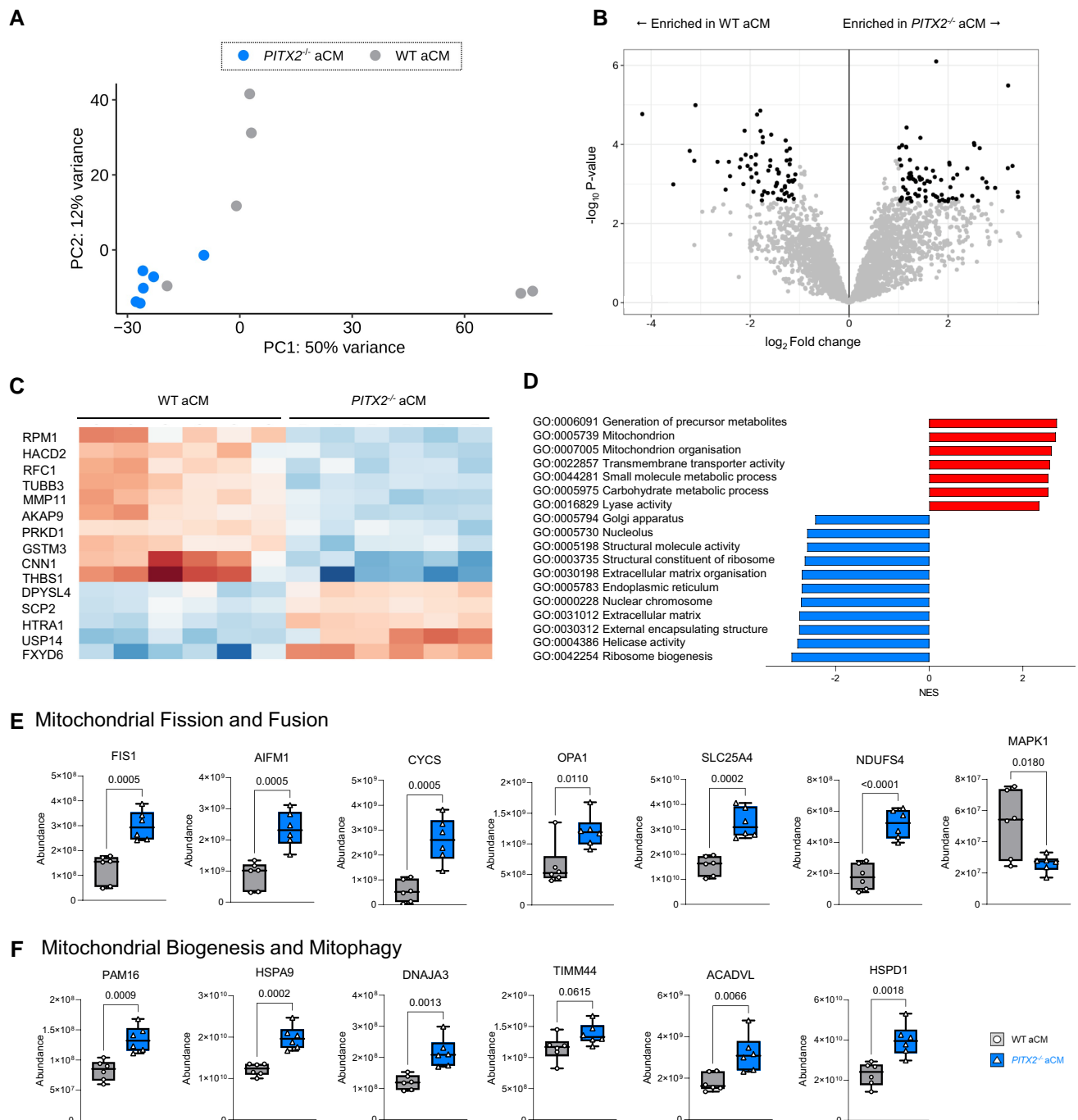


**Figure 2** Proteomic analysis of  $PITX2^{-/-}$  hiPSC-derived atrial cardiomyocytes (aCMs). (A) Principal component analysis (PCA) of samples used in proteomic analysis. (B) Volcano plot showing protein enriched in WT aCMs vs.  $PITX2^{-/-}$  aCMs. Significantly enriched proteins ( $\log_2 FC > 1$ ) are shown in black. (C) Differentially expressed mitochondrial proteins in WT aCMs and  $PITX2^{-/-}$  aCMs presented as a heatmap. (D) Gene-set enrichment analysis of enriched and down-regulated pathways in WT aCMs and  $PITX2^{-/-}$  aCMs. Proteins with an FDR < 0.05 and an absolute  $\log_2$ -fold-change > 1 were considered significantly changed. Further information on data analysis can be found in the [Supplementary materials](#). (E, F) Expression of proteins linked to mitochondrial fission and fusion (E) and related to mitochondrial biogenesis and mitophagy (F) in WT and  $PITX2^{-/-}$  aCMs ( $n = 6$ ).

data from  $PITX2^{-/-}$  and WT hiPSC-derived atrial cardiomyocytes showed differential expression of a large number of transcripts (Volcano plot in [Figure 3A](#)). Gene ontology analysis identified respiration as one of the main affected processes ([Figure 3B](#)). Based on Leiden-annotated UMAP clustering

six distinct cell populations were found, with 60.8% of all cells belonging to cluster C1 ([Figure 3C](#)). Cell clusters C1, 2, 4, and 6 consist of both  $PITX2^{-/-}$  and WT aCM nuclei. Clusters 3 and 5, containing ~10% of cells, consist predominantly of  $PITX2^{-/-}$  aCM nuclei ([Figure 3D](#)). These results identify an

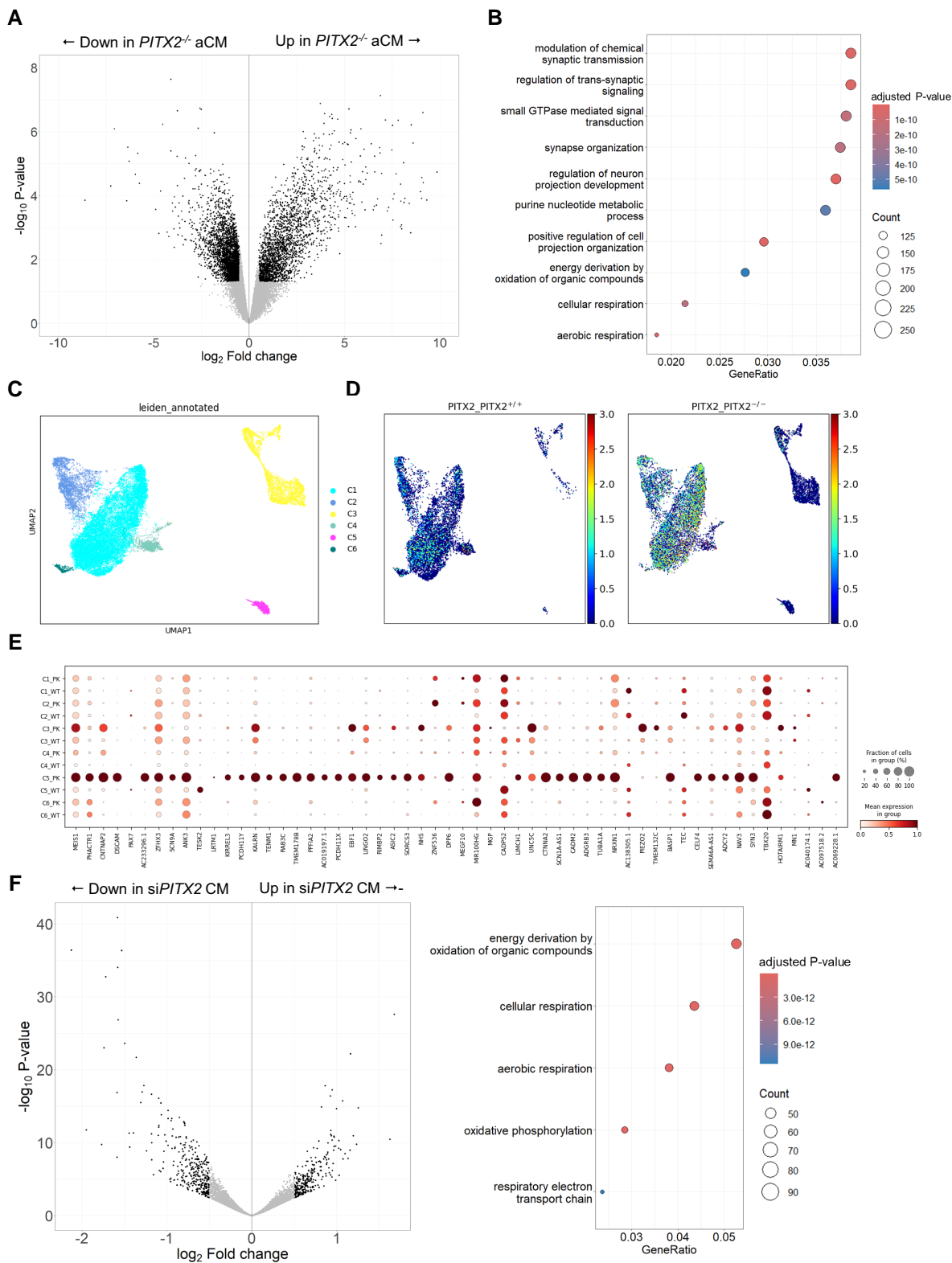


**Figure 3** Transcriptional changes in *PITX2*-deficient hiPSC-derived atrial cardiomyocytes (aCM). (A) Volcano plot of differentially expressed genes in ‘pseudo-bulk’ mRNA sequencing analysis of nuclei from *PITX2*<sup>-/-</sup> and WT control hiPSC-derived atrial cardiomyocytes. (B) Gene ontology analysis of the bulk RNA-sequencing data. (C) Leiden plot of single-nuclei RNA-sequencing identifies six clusters of cells, including one cluster containing mainly *PITX2*<sup>-/-</sup> cells. (D) Differential gene expression patterns in the single-nuclear RNA-sequencing data sets of WT (*PITX2*<sup>+/+</sup>) and *PITX2*<sup>-/-</sup> aCM depicted by cell cluster (Leiden plot). (E) List of 56 most differentially expressed genes in *PITX2*<sup>-/-</sup> hiPSC-derived atrial cardiomyocytes (PK) vs. WT based on the single-nuclear RNA-sequencing analysis. (F) Gene expression differences in a published data set<sup>36</sup> of hiPSC-derived cardiomyocytes exposed to *PITX2*-small interfering RNA (siRNA) or scrambled control siRNA. Left panel: Volcano plot. Right panel: Gene ontology analysis of differentially expressed genes.



increased heterogeneity of *PITX2*<sup>-/-</sup> hiPSC-derived atrial cardiomyocyte nuclei. Among the possible comparisons of cell lines and cells belonging to the different clusters, two were considered important: differences between genotypes in the largest cluster (C1) and differentially expressed genes in the *PITX2*<sup>-/-</sup>-enriched cluster (C3) compared with the main WT cluster (C1). Among the top differentially expressed genes between WT and *PITX2*<sup>-/-</sup> hiPSC-derived atrial cardiomyocytes in cell cluster C1 were the mitochondrial genes *COX6a* and *ABCA1* and the sodium channel *SCN9A*. Among the top differentially expressed genes between *PITX2*<sup>-/-</sup> of C1 and *PITX2*<sup>-/-</sup> of C3 were cell-cell contact and structural proteins and transcription factors (Figure 3E). Analysis of published<sup>36</sup> gene expression data in hiPSC-derived ventricular-like cardiomyocytes exposed to *PITX2*-repressing RNA or scrambled control RNA identified similar pathways regulated in response to *PITX2* repression using gene ontology (Figure 3F).

### 3.4 Changes in metabolism and mitochondrial function in *PITX2*-deficient hiPSC-derived atrial cardiomyocytes

Electron microscopy revealed no overt morphological defects between *PITX2*<sup>-/-</sup> hiPSC-derived atrial cardiomyocytes and WT controls. However, mitochondria in *PITX2*<sup>-/-</sup> hiPSC-derived atrial cardiomyocytes were smaller and less structured: some mitochondria showed a fractured outer membrane. Mitochondria in WT cells appeared elongated with visible cristae (Figure 4A). Expression of *FOXO1*, *PPARGC1a*, and *PYGM* was increased in *PITX2*<sup>-/-</sup> hiPSC-derived atrial cardiomyocytes compared with WT controls (Figure 4B), suggesting increased glycolytic activity. Seahorse experiments confirmed increased glycolysis in *PITX2*<sup>-/-</sup> hiPSC-derived atrial cardiomyocytes (Figure 4C and D). *PITX2*<sup>-/-</sup> hiPSC-derived atrial cardiomyocytes showed decreased *SLC27A6* expression (Figure 4E).

The mitochondrial/nuclear DNA ratio showed no difference between WT and *PITX2*<sup>-/-</sup> hiPSC-derived atrial cardiomyocytes (Figure 5A). *PITX2*<sup>-/-</sup> hiPSC-derived atrial cardiomyocytes showed more mitochondrial membrane content by TOMM20 flow cytometry (Figure 5B). RT-qPCR of common mitochondrial genes revealed increased *COX7C* and reduced *MCU* expression in *PITX2*<sup>-/-</sup> hiPSC-derived atrial cardiomyocytes (Figure 5C). Functional analysis of mitochondrial respiration revealed lower basal and maximal mitochondrial respiration in *PITX2*<sup>-/-</sup> hiPSC-derived atrial cardiomyocytes without changes in proton leak and oligomycin-sensitive ATP generation (Figure 5D and E). These experiments also found a higher glycolytic index in *PITX2*<sup>-/-</sup> hiPSC-derived atrial cardiomyocytes (Figure 5F). Basal mitochondrial membrane potential was higher compared with WT control cells, suggesting that *PITX2*<sup>-/-</sup> hiPSC-derived atrial cardiomyocytes already exhibit a more glycolytic metabolic state under normal culture conditions. Mitochondrial membrane potential (Figure 5G) was more sensitive to Oligomycin A in WT than in *PITX2*<sup>-/-</sup> hiPSC-derived atrial cardiomyocytes. Representative fluorescent microscopy images for TMRM and MitoTrackerGreen for both genotypes are shown (Figure 5H). Together, these results suggest that *PITX2* deficiency causes a metabolic shift to glycolysis in hiPSC-derived atrial cardiomyocytes. *PITX2*<sup>-/-</sup> hiPSC-derived atrial cardiomyocytes increase their number of mitochondria, likely to compensate for the less efficient energy generation.

### 3.5 Faster beating rates and more heterogeneous and prolonged atrial APs in *PITX2*-deficient hiPSC-derived atrial cardiomyocytes

As expected from *Pitx2*-dependent suppression of pacemaker activity in the murine left atrium,<sup>45</sup> spontaneously beating *PITX2*<sup>-/-</sup> hiPSC-derived atrial cardiomyocytes showed an increased beating frequency compared with WT hiPSC-derived atrial cardiomyocytes (Figure 6A). Concentrations of the sino-atrial node gene *SHOX2* and the myocardial gene *NKX2-5* were increased in *PITX2*<sup>-/-</sup> hiPSC-derived atrial cardiomyocytes (Figure 6B). To compare AP morphologies, we applied unbiased clustering to all AP waveforms recorded in WT and *PITX2*<sup>-/-</sup> hiPSC-derived atrial cardiomyocytes (Figure 6C). Atrial AP clustered into three distinct morphologies (clusters

1–3). *PITX2*<sup>-/-</sup> hiPSC-derived atrial cardiomyocytes consistently showed more AP waveforms belonging to ‘cluster 3’ APs (with prolonged APs) compared with WT hiPSC-derived atrial cardiomyocytes during pacing and spontaneous beating (Figure 6C and [Supplementary material online, Table S6](#)). The additional AP morphology is one of the reasons why, on average, *PITX2*<sup>-/-</sup> hiPSC-derived atrial cardiomyocytes showed prolonged AP durations (APD, Figure 6D and [Supplementary material online, Figure S3A and B](#)). AP amplitude (Figure 6E) and peak upstroke velocity ( $dV/dt_{max}$ ) hiPSC-derived atrial cardiomyocytes (Figure 6G) were reduced in *PITX2*<sup>-/-</sup> hiPSC-derived atrial cardiomyocytes compared with WT. The diastolic membrane potential was variable, but not different between genotypes (Figure 6F and G). These electrophysiological changes were less pronounced at high pacing rates (2 and 3 Hz, [Supplementary material online, Figure S3C–E](#)). Exclusion of more depolarized, less normal-appearing APs prior to clustering led to almost identical results (data on file). *PITX2*<sup>-/-</sup> hiPSC-derived atrial cardiomyocytes showed reduced *KCNA5* expression and increased *KCNA4* and *KCNH2* gene expression (Figure 6H). Protein concentrations of *KCNA5* and *hERG* were reduced in *PITX2*<sup>-/-</sup> hiPSC-derived atrial cardiomyocytes, and *Kv1.4* concentrations were increased (Figure 6I).

### 3.6 Differential expression of metabolic genes in left atrial tissue from patients with AF

RNA-sequencing data in left atrial appendage tissue collected from 85 patients during open-heart surgery were compared between patients in SR without a diagnosis of AF (‘SR’) and patients with AF diagnosed prior to surgery and in AF during tissue collection (Figure 7A, clinical details in [Supplementary material online, Figure S4A–B](#)). Gene enrichment analysis identified 1150 up-regulated genes in left atrial appendage tissue from patients with AF compared with patients in SR (Figure 7A). Biological processes linked to mitochondrial organization, ion transport, and muscle contraction were up-regulated in AF patients (see [Supplementary material online, Figure S4C and Tables S7 and S8](#)). *COX7A1* gene expression was up-regulated and *SLC25A4* gene expression was down-regulated in atrial tissue from patients with AF compared with patients in SR (Figure 7C).

A detailed analysis of genes that surround the chromosome 4q25 locus topological associating domain identified only reduced *PITX2* in left atria from patients in AF when compared with patients in SR (see [Supplementary material online, Figure S4D](#)). Five up-regulated genes and 14 down-regulated genes were also found to be regulated in both the human left atrial RNAseq and the *PITX2*<sup>-/-</sup> hiPSC-derived atrial cardiomyocyte proteomic data sets (see [Supplementary material online, Figure S5A](#)). Integrated analysis using our proteomics data set and two published data sets of *PITX2*-deficient heart tissue from zebrafish and mice revealed nine common genes up-regulated and eight common genes down-regulated in *PITX2*<sup>-/-</sup> hiPSC-derived atrial cardiomyocytes and *Pitx2*<sup>-/-</sup> heart tissue (see [Supplementary material online, Figures S5B and S3C](#)).

### 3.7 Association of *PITX2* with metabolic and ion channel genes in human left atria with AF

Three genes implicated in glycolytic metabolism were associated with *PITX2* expression in both AF patients and *PITX2*<sup>-/-</sup> hiPSC-derived atrial cardiomyocytes (*SLC27A6*, forkhead box protein O1 (*FOXO1*) and glycogen phosphorylase (*PYGM*) Figure 7D). Consistent with findings in *PITX2*<sup>-/-</sup> hiPSC-derived atrial cardiomyocytes, *COX7C* expression was positively associated with *PITX2* expression (Figure 7E). The *PITX2* correlation of *MYH6* and *TNNT2* was also replicated in human atrial tissue (Figure 7F). Genes implicated in cell cycling and quiescence (*CCNA1*, *CCNB1*, and *HES1*) showed no correlation with *PITX2* in AF patients (see [Supplementary material online, Figure S6A](#)). The ion channel genes *KCNA5* and *KCNH2* were associated with *PITX2*, consistent with findings in *PITX2*<sup>-/-</sup> hiPSC-derived atrial cardiomyocytes (see [Supplementary material online, Figure S6B](#)). Exploratory analyses of the human LA appendage RNAseq data set and proteomic data from *PITX2*<sup>-/-</sup> hiPSC-derived atrial cardiomyocytes replicated differences in the expression of genes required for mitochondrial oxidative processes and ATP generation

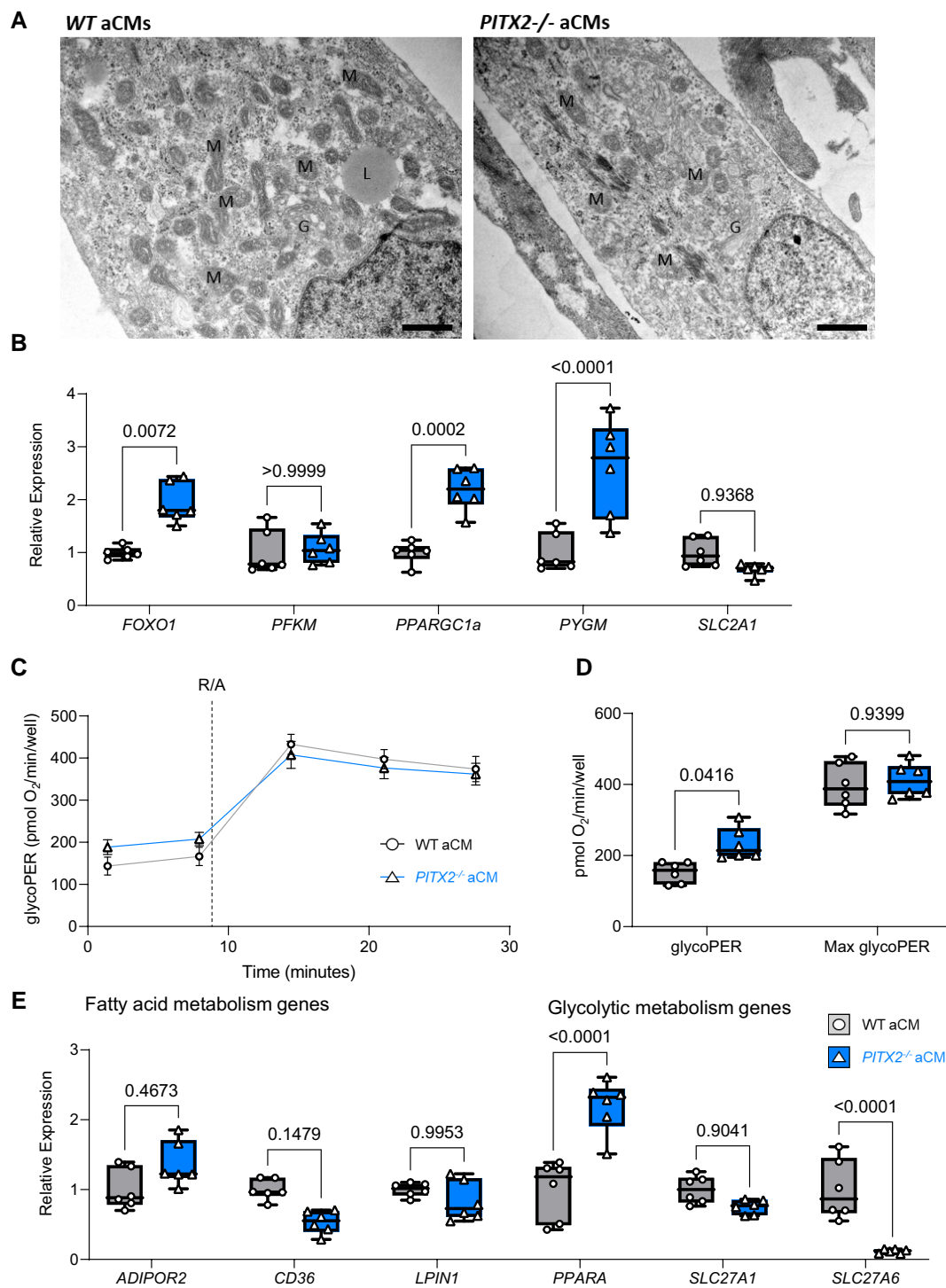


**Figure 4** Glycolytic metabolism in *PITX2*<sup>-/-</sup> hiPSC-derived atrial cardiomyocytes (aCMs). (A) Electron microscopy revealed no overt morphological differences between genotypes. Mitochondria appeared elongated and structured in WT aCMs, while they were smaller with in part fractured outer membranes in *PITX2*<sup>-/-</sup> aCMs. G: golgi; L: lipid droplet; M: mitochondria; scale bar 500 nm. (B) Gene expression of *FOXO1*, *PFKM*, *PPARGC1a*, *PYGM* and *SLC2A1* in WT and *PITX2*<sup>-/-</sup> aCMs ( $n = 6$ ) as assessed by qRT-PCR. Data are expressed as the mean relative expression and presented as box and whisker plots (min to max). (C) Measurement of glycolysis (glycoPER) as assessed by Seahorse measurements ( $n = 6$ ). Traces shown are PER corrected after subtracting non-glycolytic acidification from the rates post 2-DE addition and mitochondrial acidification contributions.<sup>29,30</sup> For representation purposes, oligomycin A and BAM addition have been removed from the trace as these are not relevant to the glycolytic measurements reported. (D) Quantification of basal glycolysis (glycoPER) and maximal glycolysis (Max glycoPER). (E) Gene expression of *ADIPOR2*, *CD36*, *LPIN1*, *PPARA*, *SLC27A1* and *SLC27A6* in WT and *PITX2*<sup>-/-</sup> aCMs ( $n = 6$ ) as assessed by qRT-PCR. Data are expressed as the mean relative values and presented as box and whisker plots (min to max). Statistical analyses were carried out using Mann–Whitney *U* tests to compare between two groups.

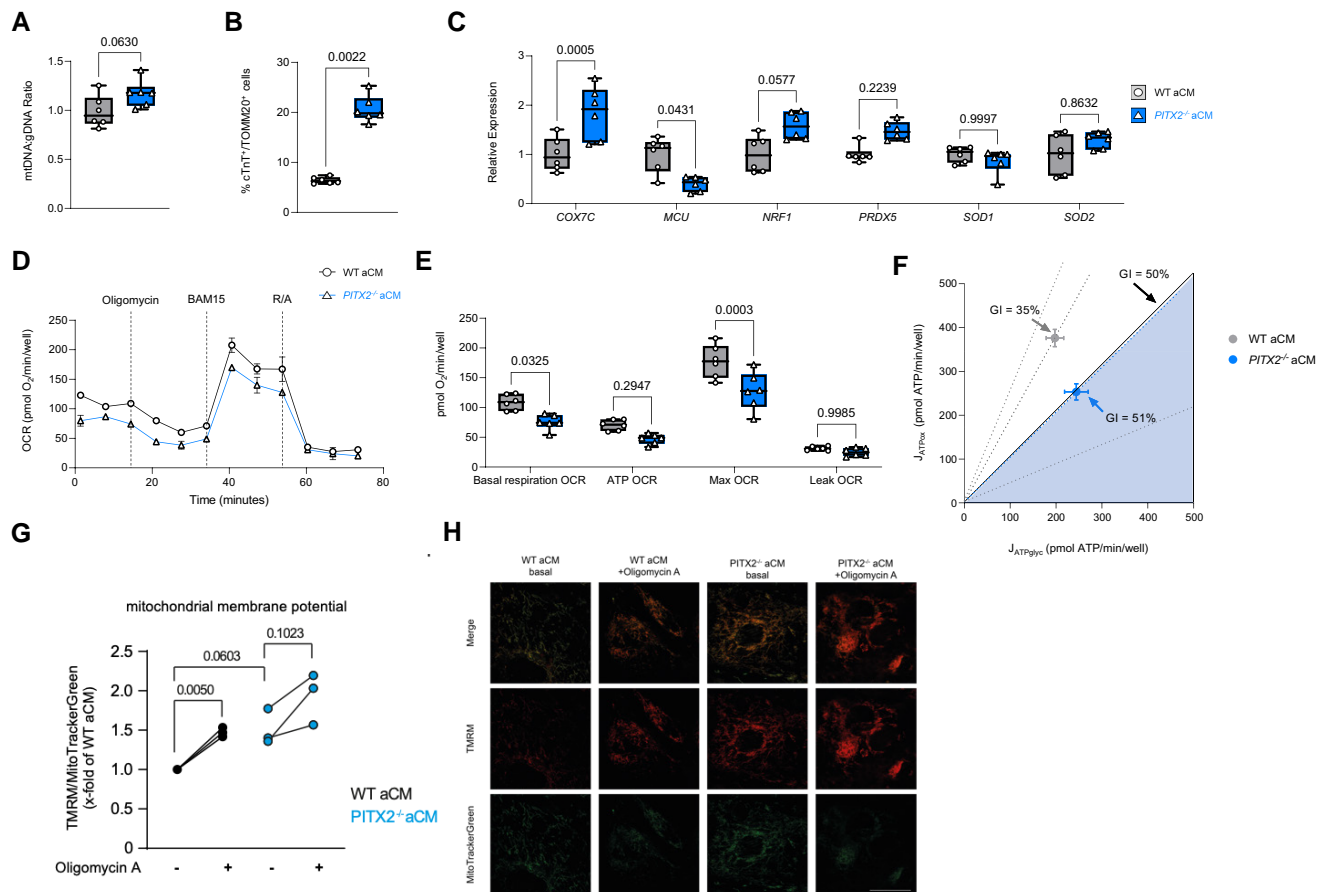


**Figure 5** Mitochondrial respiration in *PITX2*<sup>-/-</sup> hiPSC-derived atrial cardiomyocytes (aCMs). (A) Mitochondrial (ND1) to nuclear DNA (B2M) ratio as assessed by RT-qPCR (*n* = 6). (B) Flow cytometry analysis of mitochondrial membrane content in WT and *PITX2*<sup>-/-</sup> aCMs using TOMM20 staining (*n* = 6). (C) Gene expression of *COX7C*, *MCU*, *NRF1*, *PRDX5*, *SOD1* and *SOD2* in WT and *PITX2*<sup>-/-</sup> aCMs (*n* = 6) as assessed by RT-qPCR. (D) Traces showing oxygen consumption rates (OCR) in WT and *PITX2*<sup>-/-</sup> aCMs (*n* = 6). (E) Quantification of OCRs shown in (D). (F) Quantification of J<sub>ATP</sub> from either oxidative phosphorylation or glycolytic sources. Data are expressed as glycolytic indexes (GI) showing absolute values of ATP supply. (G) aCMs were loaded with the mitochondrial membrane-sensitive dye tetramethylrhodamine methyl ester (TMRM) and MitoTrackerGreen as a mitochondrial-selective loading control. Subsequently, aCMs were exposed to oligomycin A (2 μM for 10 min). Alterations in mitochondrial membrane potential of *PITX2*<sup>-/-</sup> aCMs (blue) or the isogenic control cells (wild-type WT; black) at baseline (–) or in response to oligomycin A (+) were expressed as the ratio of TMRM/MitoTrackerGreen fluorescence as fold change of the WT. The graph represents the data summarized from three independent experiments of at least 20 images per experiment from three independent aCM differentiation runs. One-way ANOVA with Sidak post-test for multiple comparisons was performed. (H) Exemplary fluorescence images used to generate the mitochondrial potential data shown in Figure 5G. Scale bar indicates 25 μm.

(see [Supplementary material online, Figure S7](#)). Overall, these associations support a role for *PITX2*-dependent regulation of oxidative phosphorylation, mitochondrial structure and function, and cardiac ion channels in patients with AF.

## 4. Discussion

### 4.1 Main findings

*PITX2* deficiency reduces mitochondrial respiration and induces a metabolic shift towards enhanced glycolysis in hiPSC-derived atrial cardiomyocytes. Similar results can be replicated in human left atria with AF. In addition, *PITX2* deficiency affects metabolic and respiratory pathways in hiPSC-derived atrial cardiomyocytes and increases heterogeneity of nuclear RNA expression. These *PITX2*-dependent effects can interact and contribute to the structural and functional changes found in *PITX2*-deficient atria and lead to AF. Our results suggest a potential effect of metabolic interventions to prevent and treat *PITX2*-dependent atrial defects and AF.

### 4.2 *PITX2*-dependent mitochondrial and metabolic dysfunction

*PITX2* deficiency led to altered protein and gene expression (Figures 2–4) that include reduced mitochondrial respiration and a metabolic shift towards increased glycolysis in atrial cardiomyocytes (Figures 4 and 5). Such defects and the resulting metabolic dysfunction can lead to fatty deposits,<sup>46,47</sup> promote fibrosis,<sup>48</sup> and underlie sarcomeric dysfunction (Figure 1, similar findings in<sup>21</sup>) in experimental AF,<sup>49</sup> thereby contributing to three key features of AF. A similar FOXO-dependent metabolic switch has been described in *PITX2*-deficient skeletal muscle.<sup>50</sup> Differential expression of metabolic genes was confirmed in human left atrial tissue (Figure 7). Single-cell nuclear RNA-sequencing identified an additional cell cluster in *PITX2*<sup>-/-</sup> CMs (Figure 3C and D) that can further add to electrical heterogeneity (Figure 6). Our findings are consistent with the role of *PITX2* in the maintenance of mitochondrial structure and function and in the regulation of mitochondrial genes in the murine heart suggested by

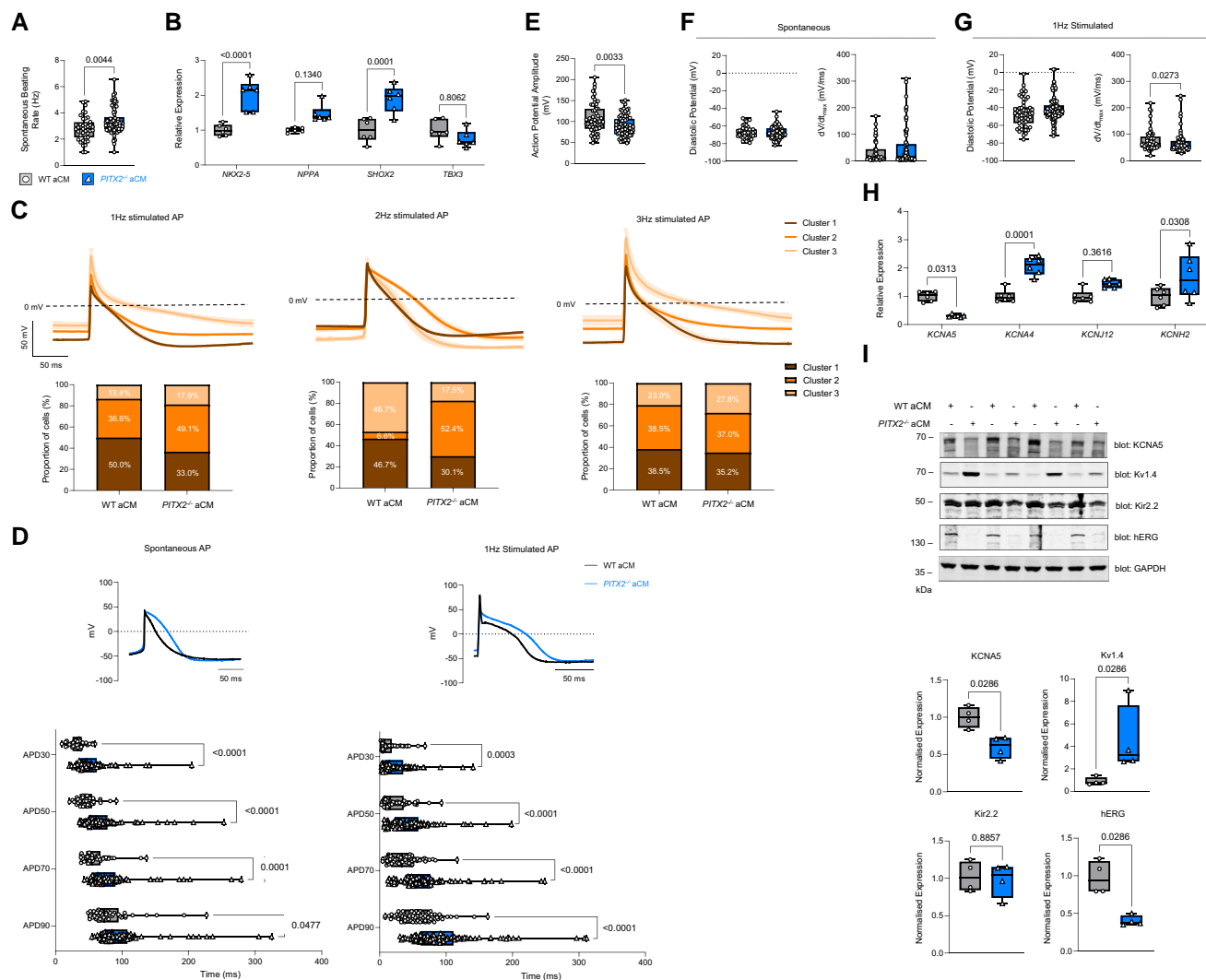


**Figure 6** Electrophysiological characterization of *PITX2*<sup>-/-</sup> hiPSC-derived atrial cardiomyocytes (aCMs). (A) Spontaneous beating rate in WT and *PITX2*<sup>-/-</sup> aCMs (WT *n* = 43, *PITX2*<sup>-/-</sup> *n* = 87). (B) Gene expression of *NKX2-5*, *NPPA*, *SHOX2*, and *TBX3* in WT and *PITX2*<sup>-/-</sup> aCMs (*n* = 6) as assessed by RT-qPCR. (C) Combined APs from 1, 2, and 3 Hz WT and *PITX2*<sup>-/-</sup> aCMs following unsupervised clustering categorized into three distinct clusters. Computationally modelled APs are shown (top) with the percentage of APs representative of those traces in WT and *PITX2*<sup>-/-</sup> aCMs quantified (below). (D) Representative action potential (AP) traces of spontaneously beating or 1 Hz paced WT aCMs and *PITX2*<sup>-/-</sup> aCMs using whole-cell patch-clamp (top). Quantification of action potential duration (APD) at APD30, 50, 70 and 90 in spontaneously beating or 1 Hz paced WT and *PITX2*<sup>-/-</sup> aCMs (spontaneously beating WT *n* = 43, *PITX2*<sup>-/-</sup> *n* = 87; 1 Hz WT *n* = 82, *PITX2*<sup>-/-</sup> *n* = 112 over five batches of independently differentiated cells: below). (E) Action potential amplitude (APA) in 1 Hz paced WT or *PITX2*<sup>-/-</sup> aCMs (1 Hz—WT *n* = 82, *PITX2*<sup>-/-</sup> *n* = 112). Diastolic potential and peak upstroke velocity (*dV/dt*<sub>max</sub>) in spontaneously beating (F) and 1 Hz paced (G) WT or *PITX2*<sup>-/-</sup> aCMs (spontaneously beating—WT *n* = 43, *PITX2*<sup>-/-</sup> *n* = 87; 1 Hz—WT *n* = 82, *PITX2*<sup>-/-</sup> *n* = 112). Note that only some cells showed spontaneous beating, resulting in different diastolic potential values than in paced cells. (H) Gene expression of *KCNA5*, *KCNA4*, *KCNJ12* and *KCNH2* in WT and *PITX2*<sup>-/-</sup> aCMs (*n* = 6) as assessed by RT-qPCR. (I) Western blot analysis of *KCNA5*, *Kv1.4*, *Kir2.2* and *hERG* in WT and *PITX2*<sup>-/-</sup> aCMs (*n* = 4). Western blots are shown on top with quantification below. GAPDH was used as a loading control. Data are expressed as the mean relative expression and presented as box and whisker plots (min to max). For electrophysiological analysis, statistics were carried out using a repeated measures ANOVA to compare differences in electrophysiological parameters. For gene and protein analysis, Mann–Whitney *U* tests were used to compare between two groups.

others.<sup>51,52</sup> Mitochondrial capacity in the heart declines during ageing,<sup>53</sup> leading to increased mitochondrial oxidative stress in cardiomyocytes.<sup>54</sup> Subtle *PITX2*-dependent mitochondrial defects could aggravate ageing-induced mitochondrial dysfunction and oxidative stress<sup>53,54</sup> and thereby promote AF. Further studies testing metabolic challenges in *PITX2*-deficient atrial models are warranted to unmask subtle metabolic defects and to study whether *PITX2* is involved in atrial protection against hypoxia and oxidative stress.<sup>51</sup> Our findings support the concept that metabolic

support of the atria conveys at least a part of the AF-preventing effects of SGLT2 inhibitors<sup>55,56</sup> and PARP inhibition.<sup>57</sup>

### 4.3 *PITX2*-dependent regulation of cellular function and metabolic predisposition to AF

Cardiomyocyte function including ion homeostasis requires sustained and high energy production. The increased heterogeneity of atrial APs (Figure 6), shorter



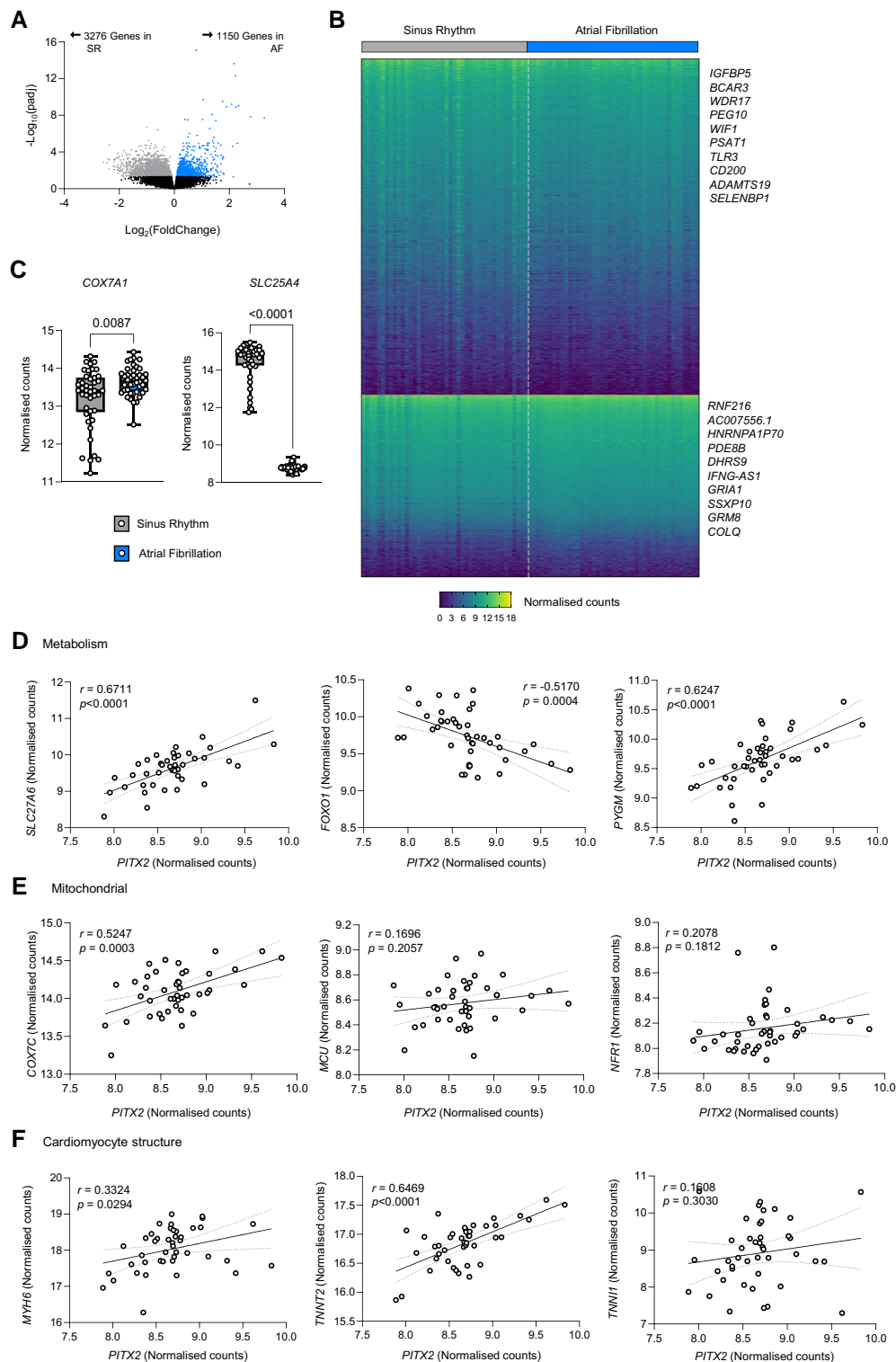


**Figure 7** Bulk RNA-sequencing of left atrial appendage tissue from AF and SR patients. Left atrial tissue was collected during open-heart surgery from patients with known AF and in sinus rhythm (SR) during the operation ('SR') and from patients with permanent AF including during surgery. (A) Volcano plot showing genes in patients with AF (permanent AF) vs. those in SR at the time of tissue harvest. Significantly enriched genes [false discovery rate (FDR) < 0.05] in AF patients (blue) and significantly enriched genes in SR patients (grey) are shown. (B) Differentially expressed genes in individual samples of patients in SR and AF. Selected genes represent the top 10 enriched genes in either SR patients (top) or AF patients (bottom). (C) Expression of *COX7A1* and *SLC25A4* in sinus rhythm (SR) and permanent AF patients' atrial tissue (Sinus rhythm  $n = 42$ ; AF  $n = 43$ ). Correlation analysis of *PITX2*-regulated genes in patients with chronic (permanent) AF implicated in (D) metabolism (*SLC27A6*, *FOXO1*, and *PYGM*), (E) mitochondrial function (*COX7C*, *MCU*, and *NRF1*) and (F) cardiomyocyte structure (*MYH6*, *TNNT2*, and *TNNI1*). Data represent  $n = 43$  with Spearman  $r$  values and corrected  $P$ -values shown on graph.

sarcomeres (Figure 1), and contractile dysfunction<sup>49</sup> seen in *PITX2*<sup>-/-</sup> hiPSC-derived atrial cardiomyocytes and in other models of *PITX2* deficiency in mice<sup>20,22</sup> can be caused by mitochondrial dysfunction altering atrial calcium handling<sup>58–61</sup> and repolarization,<sup>62</sup> in addition to direct, *PITX2*-dependent regulation of ion channel expression (see [Supplementary material online, Figure S6](#)). The pathway analyses in *PITX2*<sup>-/-</sup> hiPSC-derived atrial cardiomyocytes and of published data in cardiomyocytes with post-differentiation repression of *PITX2* (Figure 3) show dysregulation of metabolic and mitochondrial respiration, suggesting that metabolic dysfunction is one of the main changes associated with *PITX2* deficiency in cardiomyocytes. The increased functional heterogeneity in *PITX2*<sup>-/-</sup> hiPSC-derived atrial cardiomyocytes may also reflect the effects of an additional cell cluster found by single-nuclear sequencing (Figure 3). Future interventional studies aiming at restoring mitochondrial function can determine the role of metabolic dysfunction in these *PITX2*-dependent changes. Structural defects have been described in conditionally *PITX2*-deficient hearts before.<sup>20</sup> This study finds structural defects in *PITX2*-deficient hiPSC-derived atrial cardiomyocytes kept in culture, showing a direct effect of *PITX2* deficiency on structural alterations in the heart. Combined *PITX2*<sup>-/-</sup> hiPSC-derived atrial cardiomyocytes proteomics, single-nuclear RNA-sequencing and analysis of human atrial RNA-sequencing identified *PITX2*-regulated ion channel and mitochondrial genes. Changes in mitochondrial genes are consistent with recent RNAseq data sets in animal models of AF,<sup>63</sup> and in patients with AF (*ETFB* gene).<sup>64</sup> Correlation of *PITX2* gene expression and metabolic gene expression in atria from patients with AF (Figure 7), dysregulation in *PITX2*-deficient hiPSC-derived atrial cardiomyocytes (Figure 3) and changes in cardiomyocytes exposed to *PITX2* siRNA (Figure 3) support metabolic gene regulation by *PITX2*. Compared with the shortening of atrial APs in murine models of *Pitx2* deficiency,<sup>12,18</sup> the AP prolongation observed in this study (Figure 6) was unexpected. The increased heterogeneity of early repolarisation found here is consistent with *PITX2*-deficiency-dependent electrophysiological changes in another, independently generated *PITX2*-deficient hiPSC-derived atrial cardiomyocyte model.<sup>19</sup> Metabolic and other *PITX2*-dependent effects and inter-species variability may contribute to these differences. The more subtle electrical phenotype in heterozygous *Pitx2*-deficient (*Pitx2c*<sup>+/-</sup>) mice<sup>12,16–18</sup> is consistent with a less profound, dose-dependent defect. Key next steps to better understand the interactions between mitochondrial and metabolic state, gene expression, cardiomyocyte structure, ion channel dysregulation, and altered atrial electrophysiology are metabolic challenges and interventions aiming to restore mitochondrial function to assess the resulting phenotypic changes and

a role of *PITX2*. Our findings suggest that therapies improving cardiomyocyte metabolism could help to prevent AF linked to *PITX2*. The prevention of AF by SGLT2 inhibitors<sup>55,65</sup> is a clear clinical sign that metabolic interventions have potential for AF treatment.

## 4.4 Strengths and limitations

Strengths of the study are a human aCM model enabling the observation of structural and functional *PITX2*-dependent changes in atrial cardiomyocytes in the absence of arrhythmias and other cardiovascular stressors, the hypothesis-generating characterization of the hiPSC-derived atrial cardiomyocytes and the confirmation of key findings in human atria with AF. Independent validation in hiPSC-derived cardiomyocytes and in other experimental and clinical models is desirable, including in organoid models and animals with left and right atria. Our single-nuclei RNA-sequencing analysis confirms metabolic changes and finds an increased cellular heterogeneity affecting ~10% of cells. This illustrates the multifaceted effects of suppression of *PITX2* in cardiomyocytes. Future research is needed to define potential dose-dependent, milder metabolic phenotypes in other *PITX2*-deficient cells and animal models.<sup>12,16–18</sup> Further research is also needed to identify the mechanisms of mitochondrial dysfunction and to identify potential therapeutic targets. Putative crosstalk between cardiomyocytes and other atrial cells requires further studies in multicellular hiPSC-derived, animal, and human models. Another limitation is the relatively high variability of electrical function in the hiPSC-derived atrial cardiomyocytes<sup>19</sup> which reflects different cell clusters and variable maturation.<sup>66</sup> This variability may have obviated subtle differences, e.g. in diastolic potential, between genotypes. Improved hiPSC-atrial cardiomyocyte maturation using engineered heart tissue<sup>19</sup> and three-dimensional growth techniques<sup>67</sup> may generate more mature cells and organoids suitable to address these questions. Finally, although RNA-sequencing of left atrial appendages enabled us to evaluate *PITX2*'s function in patients, these analyses were limited to bulk sequencing of atrial tissue obtained during open-heart surgery. Limited access to cardiac tissue outside of surgical procedures renders this limitation difficult to overcome. The single-nuclei sequencing removed mitochondria prior to sequencing. Genes encoded by mitochondrial DNA (13 genes) were not included in the single-nuclear sequencing analyses. In view of the large number of mitochondrial genes encoded by nuclear DNA, this is a minor limitation in our view.

## Translational perspective

The strongest genetic predisposition for AF is located on chromosome 4q25, close to the *PITX2* gene. This study in human iPS-derived atrial cardiomyocytes shows that deletion of *PITX2* leads to genetic and proteomic changes resulting in metabolic and mitochondrial dysfunction in atrial cardiomyocytes. Similar *PITX2*-dependent changes are found in human left atria. Our results identify metabolic and mitochondrial dysfunction as a novel contributor to AF in patients with a genetic predisposition. They support the evaluation of metabolic therapies to prevent and reverse functional and structural defects related to AF and its genetic basis.

## Supplementary material

[Supplementary material](#) is available at *Cardiovascular Research* online.

## Author contributions

Conception and design of the research: J.S.R., P.K., L.F.; acquisition of data: J.S.R., L.C.S., M.o.R., V.R.C., A.O.K., S.H., C.M., J.B., O.H., N.H., R.J.S., S.N.K., O.G., M.S., T.B., F.C., A.P.; analysis and interpretation of the data: J.S.R., L.C.S., M.o.R., V.R.C., E.T., A.O.K., C.o.S., S.H., N.H., O.H., C.M., M.S., A.P., J.B., T.B., K.L., F.C.; statistical analysis: J.S.R., V.R.C., J.B., W.C., J.W., T.B., C.L., F.C., S.Z.; supervising the experiments: J.S.R., F.C., P.K., L.F.;

drafting the manuscript: J.S.R., P.K., L.F.; critical revision of the manuscript for important intellectual content: L.C.S., W.C., S.K., L.M., S.N.H., N.V.M., J.R., K.G., K.L., F.C., M.St., U.S., G.V.G. All authors approve the current version of the manuscript.

## Acknowledgements

We would like to thank Boris Greber for providing the hiPSC lines used in this study and Daniela Moralli (University of Oxford Karyotyping Core Facility) who assisted with karyotyping analysis. The Seahorse Extracellular Flux analysis was supported by the Cellular Health and Metabolism Facility in the College of Life and Environmental Sciences at the University of Birmingham. In addition, we would like to thank

the Translational Research on Heart Failure and Arrhythmias Cluster, ICVS Birmingham for useful insights and thoughtful discussions on the manuscript.

**Conflict of interest:** L.F. has received institutional research grants and non-financial support from European Union, British Heart Foundation, Medical Research Council (U.K.), DFG, German Centre for Heart Research DZHK and several biomedical companies. P.K. has received additional support for research from the European Union, British Heart Foundation, Foundation Leducq, Medical Research Council (U.K.), and German Centre for Cardiovascular Research, from several drug and device companies active in AF, Honoria from several such companies, but not in the last three years. P.K. and L.F. are listed as inventors on two patents held by University of Birmingham (AFTherapy WO 2015140571, Markers for AF WO 2016021783). U.S. has received consultancy fees or honoraria from Università della Svizzera Italiana (USI, Switzerland), Roche Diagnostics (Switzerland), EP Solutions Inc. (Switzerland), Johnson & Johnson Medical Limited, (U.K.), Bayer Healthcare (Germany). U.S. is co-founder and shareholder of YourRhythmics BV, a spin-off company of the University Maastricht. K.G. has received additional support for research from the British Heart Foundation, Medical Research Council (U.K.), and Rocket Pharmaceuticals Inc. All other authors declare they have no competing interests.

## Funding

This work was supported by the European Commission (grant agreements no. 633196 [CATCH ME]) to P.K., L.F., M.S. and U.S. no. 116074 [BigData@Heart EU MI] to P.K., no. 985286 [MAESTRIA] to L.F., U.S., British Heart Foundation (FS/13/43/30324 and AA/18/2/34218 to P.K. and L.F.), German Centre for Cardiovascular Research supported by the German Ministry of Education and Research (DZHK, to P.K. and L.F.), Foundation Leducq (140VD01) to P.K. and Deutsche Forschungsgemeinschaft (DFG, 509167694; KI73/4-1) to P.K. and (CU53/5-1; CU53/10-1; CU53/12-1) to FC, and SFB1525/453989101 and SFB/TR 296/424957847 to K.L. J.S.R. and K.G. acknowledge support from a British Heart Foundation Accelerator Award (AA/18/2/34218). K.G. is supported by the Medical Research Council (MR/V009540/1) and the National Centre for the Replacement, Refinement and Reduction of Animals in Research (NC/T001747/1). A.O.K. and C.o.S. are Sir Henry Wellcome Fellows (218649/Z/19/Z; 221650/Z/20/Z). J.R. is a British Heart Foundation Intermediate Fellow (FS/IBSRF/20/25039). U.S. is supported by grants from the Netherlands Heart Foundation (CVON2014-09 [RACE-V] and grant number 01-002-2022-0118, EmBRACE) and the European Commission (no. 860974 [ITN Network Personalise AF] and no. 952166 [REPAIR]). NH is supported by the DFG SFB-1470-B03, the Chan Zuckerberg Foundation, and an ERC Advanced Grant under the European Union Horizon 2020 Research and Innovation Program (AdG788970). V.R.C. and G.V.G. acknowledge support from the MRC Health Data Research UK (HDRUK/CFC/01), an initiative funded by the UK Research and Innovation, Department of Health and Social Care (England). M.O. is the recipient of a Dutch Heart Foundation Dekker grant (03-004-2022-0036) and ZonMW Off-Road research grant (04510012110049). A CC BY or equivalent license is applied to AAM arising from this submission, in accordance with the grant's open access conditions.

## Data availability

All data associated with this study are present in the paper or in the [Supplementary Materials](#). Sequencing datasets used in this study can be requested from the corresponding author. The mass spectrometry proteomics dataset has been deposited to the ProteomeXchange Consortium via the PRIDE partner repository with the dataset identifier PXD037189. The snRNA sequencing data set has been deposited in the European Nucleotide Archive (ENA) at EMBL-EBI under accession number PRJEB75160 (<https://www.ebi.ac.uk/ena/browser/view/PRJEB75160>).

## References

- Hindricks G, Potpara T, Dagres N, Arbelo E, Bax JJ, Blomstrom-Lundqvist C, Boriani G, Castella M, Dan GA, Dilaveris PE, Fauchier L, Filippatos G, Kalman JM, La Meir M, Lane DA, Lebeau JP, Lettino M, Lip GYH, Pinto FJ, Thomas GN, Valgimigli M, Van Gelder IC, Van Putte BP, Watkins CL; ESC Scientific Document Group. 2020 ESC guidelines for the diagnosis and management of atrial fibrillation developed in collaboration with the European Association for Cardio-Thoracic Surgery (EACTS): the task force for the diagnosis and management of atrial fibrillation of the European Society of Cardiology (ESC) developed with the special contribution of the European Heart Rhythm Association (EHRA) of the ESC. *Eur Heart J* 2021;**42**:373–498.
- Kirchhof P. The future of atrial fibrillation management: integrated care and stratified therapy. *Lancet* 2017;**390**:1873–1887.
- Lin Z, Andrade JG, Arbelo E, Boriani G, Breithardt G, Camm AJ, Caso V, Nielsen JC, De Melis M, De Potter T, Dichtl W, Diederichsen SZ, Dobrev D, Doll N, Duncker D, Dworatzek E, Eckardt L, Eisert C, Fabritz L, Farkowski M, Filgueiras-Rama D, Goette A, Guasch E, Hack G, Hatem S, Haeusler KG, Healey JS, Heidebuechel H, Hijazi Z, Hofmeister LH, Hove-Madsen L, Huebner T, Kaab S, Kotecha D, Malaczynska-Rajpold K, Merino JL, Metzner A, Mont L, Ng GA, Oeff M, Parwani AS, Puererfellner H, Ravens U, Rienstra M, Sanders P, Scherr D, Schnabel R, Schotten U, Sohns C, Steinbeck G, Steven D, Toennis T, Tzeis S, van Gelder IC, van Leerdam RH, Vernooy K, Wadhwa M, Wakili R, Willems S, Witt H, Zeemering S, Kirchhof P. Longer and better lives for patients with atrial fibrillation: the 9th AFNET/EHRA consensus conference. *Europace* 2024;**26**:euae070.
- Schnabel RB, Marinelli EA, Arbelo E, Boriani G, Boveda S, Buckley CM, Camm AJ, Casadei B, Chua W, Dagres N, de Melis M, Desteghe L, Diederichsen SZ, Duncker D, Eckardt L, Eisert C, Engler D, Fabritz L, Freedman B, Gillet L, Goette A, Guasch E, Svendsen JH, Hatem SN, Haeusler KG, Healey JS, Heidebuechel H, Hindricks G, Hobbs FDR, Hubner T, Kotecha D, Krekler M, Leclercq C, Lewalter T, Lin H, Linz D, Lip GYH, Lochen ML, Lucassen W, Malaczynska-Rajpold K, Massberg S, Merino JL, Meyer R, Mont L, Myers MC, Neubeck L, Niiranen T, Oeff M, Oldgren J, Potpara TS, Psaroudakis G, Puererfellner H, Ravens U, Rienstra M, Rivard L, Scherr D, Schotten U, Shah D, Sinner MF, Smolnik R, Steinbeck G, Steven D, Svennberg E, Thomas D, True Hills M, van Gelder IC, Vardar B, Pala E, Wakili R, Wegscheider K, Wieloch M, Willems S, Witt H, Ziegler A, Daniel Zink M, Kirchhof P. Early diagnosis and better rhythm management to improve outcomes in patients with atrial fibrillation: the 8th AFNET/EHRA consensus conference. *Europace* 2023;**25**:6–27.
- Gudbjartsson DF, Arnar DO, Helgadóttir A, Gretarsdóttir S, Holm H, Sigurdsson A, Jonasdóttir A, Baker A, Thorleifsson G, Kristjánsson K, Pálsson A, Blondal T, Sulem P, Backman VM, Hardarson GA, Páldóttir E, Helgason A, Sigurjonsdóttir R, Sverrisson JT, Kostulas K, Ng MC, Baum L, So WY, Wong KS, Chan JC, Furie KL, Greenberg SM, Sale M, Kelly P, MacRae CA, Smith EE, Rosand J, Hillert J, Ma RC, Ellinor PT, Thorgerusson G, Gulcher JR, Kong A, Thorsteinsdóttir U, Stefansson K. Variants conferring risk of atrial fibrillation on chromosome 4q25. *Nature* 2007;**448**:353–357.
- Ellinor PT, Lunetta KL, Albert CM, Glazer NL, Ritchie MD, Smith AV, Arking DE, Muller-Nurasyid M, Krijthe BP, Lubitz SA, Bis JC, Chung MK, Dorr M, Ozaki K, Roberts JD, Smith JG, Pfeufer A, Sinner MF, Lohman K, Ding J, Smith NL, Smith JD, Rienstra M, Rice KM, Van Wagoner DR, Magnani JW, Wakili R, Clauss S, Rotter JI, Steinbeck G, Launer LJ, Davies RW, Borkovich M, Harris TB, Lin H, Volker U, Volzke H, Milán DJ, Hofman A, Boerwinkle E, Chen LY, Soliman EZ, Voight BF, Li G, Chakravarti A, Kubo M, Tedrow UB, Rose LM, Ridker PM, Conen D, Tsunoda T, Furukawa T, Sotoodehnia N, Xu S, Kamatani N, Levy D, Nakamura Y, Parvez B, Mahida S, Furie KL, Rosand J, Muhammad R, Psaty BM, Meitinger T, Perz S, Wichmann HE, Witteman JC, Kao WH, Kathiresan S, Roden DM, Uitterlinden AG, Rivadeneira F, McKnight B, Sjogren M, Newman AB, Liu Y, Gollob MH, Melander O, Tanaka T, Stricker BH, Felix SB, Alonso A, Darbar D, Barnard J, Chasman DI, Heckbert SR, Benjamin EJ, Gudnason V, Kaab S. Meta-analysis identifies six new susceptibility loci for atrial fibrillation. *Nat Genet* 2012;**44**:670–675.
- Lubitz SA, Lunetta KL, Lin H, Arking DE, Trompet S, Li G, Krijthe BP, Chasman DI, Barnard J, Kleber ME, Dorr M, Ozaki K, Smith AV, Muller-Nurasyid M, Walter S, Agarwal SK, Bis JC, Brody JA, Chen LY, Everett BM, Ford I, Franco OH, Harris TB, Hofman A, Kaab S, Mahida S, Kathiresan S, Kubo M, Launer LJ, MacFarlane PW, Magnani JW, McKnight B, McManus DD, Peters A, Psaty BM, Rose LM, Rotter JI, Silbernagel G, Smith JD, Sotoodehnia N, Stott DJ, Taylor KD, Tomaschitz A, Tsunoda T, Uitterlinden AG, Van Wagoner DR, Volker U, Volzke H, Murabito JM, Sinner MF, Gudnason V, Felix SB, Marz W, Chung M, Albert CM, Stricker BH, Tanaka T, Heckbert SR, Jukema JW, Alonso A, Benjamin EJ, Ellinor PT. Novel genetic markers associate with atrial fibrillation risk in Europeans and Japanese. *J Am Coll Cardiol* 2014;**63**:1200–1210.
- Roselli C, Chaffin MD, Weng LC, Aeschbacher S, Ahlberg G, Albert CM, Almgren P, Alonso A, Anderson CD, Aragam KG, Arking DE, Barnard J, Bartz TM, Benjamin EJ, Bihlmeyer NA, Bis JC, Bloom HL, Boerwinkle E, Bottinger EB, Brody JA, Calkins H, Campbell A, Cappola TP, Carlquist J, Chasman DI, Chen LY, Chen YI, Choi EK, Choi SH, Christophersen IE, Chung MK, Cole JW, Conen D, Cook J, Crijns HJ, Cutler MJ, Damrauer SM, Daniels BR, Darbar D, Delgado D, Denny JC, Dichgans M, Dorr M, Dudkin EA, Dudley SC, Esa N, Esko T, Eskola M, Fatkin D, Felix SB, Ford I, Franco OH, Geelhoed B, Grewal RP, Gudnason V, Guo X, Gupta N, Gustafsson S, Gutmann R, Hamsten A, Harris TB, Hayward C, Heckbert SR, Hernesniemi J, Hocking LJ, Hofman A, Horimoto A, Huang J, Huang PL, Huffman J, Ingelsson E, Ipek EG, Ito K, Jimenez-Conde J, Johnson R, Jukema JW, Kaab S, Kahonen M, Kamatani Y, Kane JP, Kastrati A, Kathiresan S, Katschnig-Winter P, Kavousi M, Kessler T, Kietselaer BL, Kirchhof P, Kleber ME, Knight S, Krieger JE, Kubo M, Launer LJ, Laurikka J, Lehtimäki T, Leineweber K, Lemaitre RN, Li M, Lim HE, Lin HJ, Lin H, Lind



- L, Lindgren CM, Lokki ML, London B, Loos RJF, Low SK, Lu Y, Lyytikäinen LP, Macfarlane PW, Magnusson PK, Mahajan A, Malik R, Mansur AJ, Marcus GM, Margolin L, Margulies KB, Marz W, McManus DD, Melander O, Mohanty S, Montgomery JA, Morley MP, Morris AP, Muller-Nurasyid M, Natale A, Nazarian S, Neumann B, Newton-Cheh C, Niemeijer MN, Nikus K, Nilsson P, Noordam R, Oellers H, Olesen HS, Orho-Melander M, Padmanabhan S, Pak HN, Pare G, Pedersen NL, Pera J, Pereira A, Porteous D, Psaty BM, Pulit SL, Pullinger CR, Rader DJ, Refsgaard L, Ribases M, Ridker PM, Rienstra M, Risch L, Roden DM, Rosand J, Rosenberg MA, Rost N, Rotter JJ, Saba S, Sandhu RK, Schnabel RB, Schramm K, Schunkert H, Schurman C, Scott SA, Seppala I, Shaffer C, Shah S, Shalaby AA, Shim J, Shoemaker MB, Siland JE, Sinisalo J, Sinner MF, Slowik A, Smith AV, Smith BH, Smith JG, Smith JD, Smith NL, Soliman EZ, Sotoodehnia N, Stricker BH, Sun A, Sun H, Svendsen JH, Tanaka T, Tanriverdi K, Taylor KD, Teder-Laving M, Teumer A, Theriault S, Trompet S, Tucker NR, Tveit A, Uitterlinden AG, Van Der Harst P, Van Gelder IC, Van Wagoner DR, Verweij N, Vlachopoulou E, Volker U, Wang B, Weeke PE, Weijs B, Weiss R, Weiss S, Wells QS, Wiggins KL, Wong JA, Woo D, Worrall BB, Yang PS, Yao J, Yoneda ZT, Zeller T, Zeng L, Lubitz SA, Lunetta KL, Ellinor PT. Multi-ethnic genome-wide association study for atrial fibrillation. *Nat Genet* 2018;**50**:1225–1233.
- Zhang M, Hill MC, Kadow ZA, Suh JH, Tucker NR, Hall AW, Tran TT, Swinton PS, Leach JP, Margulies KB, Ellinor PT, Li N, Martin JF. Long-range Pitx2c enhancer-promoter interactions prevent predisposition to atrial fibrillation. *Proc Natl Acad Sci U S A* 2019;**116**:22692–22698.
- van Ouwkerk AF, Bosada F, Liu J, Zhang J, van Duijvenboden K, Chaffin M, Tucker N, Pijnappels DA, Ellinor PT, Barnett P, de Vries AA, Christoffels VM. Identification of functional variant enhancers associated with atrial fibrillation. *Circ Res* 2020;**127**:229–243.
- Aguirre LA, Alonso ME, Badia-Careaga C, Rollan I, Arias C, Fernandez-Minan A, Lopez-Jimenez E, Aranega A, Gomez-Skarmeta JL, Franco D, Manzanares M. Long-range regulatory interactions at the 4q25 atrial fibrillation risk locus involve PITX2c and ENPEP. *BMC Biol* 2015;**13**:26.
- Kirchhof P, Kahr PC, Kaese S, Piccini I, Vokshi I, Scheld HH, Rotering H, Fortmueller L, Laakmann S, Verheule S, Schotten U, Fabritz L, Brown NA. PITX2c is expressed in the adult left atrium, and reducing Pitx2c expression promotes atrial fibrillation inducibility and complex changes in gene expression. *Circ Cardiovasc Genet* 2011;**4**:123–133.
- Reyat JS, Chua W, Cardoso VR, Witten A, Kastner PM, Kabir SN, Sinner MF, Wesselink R, Holmes AP, Pavlovic D, Stoll M, Kaab S, Gkoutos GV, de Groot JR, Kirchhof P, Fabritz L. Reduced left atrial cardiomyocyte PITX2 and elevated circulating BMP10 predict atrial fibrillation after ablation. *JCI Insight* 2020;**5**:e139179.
- Kahr PC, Piccini I, Fabritz L, Greber B, Scholer H, Scheld HH, Hoffmeier A, Brown NA, Kirchhof P. Systematic analysis of gene expression differences between left and right atria in different mouse strains and in human atrial tissue. *PLoS One* 2011;**6**:e26389.
- van Ouwkerk AF, Hall AW, Kadow ZA, Lazarevic S, Reyat JS, Tucker NR, Nadadur RD, Bosada FM, Bianchi V, Ellinor PT, Fabritz L, Martin JF, de Laat W, Kirchhof P, Moskowitz IP, Christoffels VM. Epigenetic and transcriptional networks underlying atrial fibrillation. *Circ Res* 2020;**127**:34–50.
- Wang J, Klysiak E, Sood S, Johnson RL, Wehrens XH, Martin JF. Pitx2 prevents susceptibility to atrial arrhythmias by inhibiting left-sided pacemaker specification. *Proc Natl Acad Sci U S A* 2010;**107**:9753–9758.
- Ammirabile G, Tessari A, Pignataro V, Szumska D, Suter Sardo F, Benes J Jr, Balistreri M, Bhattacharya S, Sedmera D, Campione M. Pitx2 confers left morphological, molecular, and functional identity to the sinus venosus myocardium. *Cardiovasc Res* 2012;**93**:291–301.
- Syeda F, Holmes AP, Yu TY, Tull S, Kuhlmann SM, Pavlovic D, Betney D, Riley G, Kucera JP, Jousset F, de Groot JR, Rohr S, Brown NA, Fabritz L, Kirchhof P. PITX2 modulates atrial membrane potential and the antiarrhythmic effects of sodium-channel blockers. *J Am Coll Cardiol* 2016;**68**:1881–1894.
- Schulz C, Lemoine MD, Mearini G, Koivumaki J, Sani J, Schwedhelm E, Kirchhof P, Ghalawini A, Stoll M, Hansen A, Eschenhagen T, Christ T. PITX2 knockout induces key findings of electrical remodeling as seen in persistent atrial fibrillation. *Circ Arrhythm Electrophysiol* 2023;**16**:e011602.
- Tessari A, Pietrobbon M, Notte A, Cifelli G, Gage PJ, Schneider MD, Lembo G, Campione M. Myocardial Pitx2 differentially regulates the left atrial identity and ventricular asymmetric remodeling programs. *Circ Res* 2008;**102**:813–822.
- Chinchilla A, Daimi H, Lozano-Velasco E, Dominguez JN, Caballero R, Delpon E, Tamargo J, Cinca J, Hove-Madsen L, Aranega AE, Franco D. PITX2 insufficiency leads to atrial electrical and structural remodeling linked to arrhythmogenesis. *Circ Cardiovasc Genet* 2011;**4**:269–279.
- Lozano-Velasco E, Hernandez-Torres F, Daimi H, Serra SA, Herraiz A, Hove-Madsen L, Aranega A, Franco D. Pitx2 impairs calcium handling in a dose-dependent manner by modulating Wnt signaling. *Cardiovasc Res* 2016;**109**:55–66.
- Marzenke M, Fell J, Piccini I, Ropke A, Seeböhm G, Greber B. Generation and cardiac subtype-specific differentiation of PITX2-deficient human iPS cell lines for exploring familial atrial fibrillation. *Stem Cell Res* 2017;**21**:26–28.
- Cyganek L, Tiburcy M, Sekeres K, Gerstenberg K, Bohnenberger H, Lenz C, Henze S, Stauske M, Salinas G, Zimmermann WH, Hasenfuss G, Guan K. Deep phenotyping of human induced pluripotent stem cell-derived atrial and ventricular cardiomyocytes. *JCI Insight* 2018;**3**:e99941.
- Devalla HD, Schwach V, Ford JW, Milnes JT, El-Haou S, Jackson C, Gkatzis K, Elliott DA, Chua de Sousa Lopes SM, Mummery CL, Verkerk AO, Passier R. Atrial-like cardiomyocytes from human pluripotent stem cells are a robust preclinical model for assessing atrial-selective pharmacology. *EMBO Mol Med* 2015;**7**:394–410.
- Morris TA, Naik J, Fibben KS, Kong X, Kiyono T, Yokomori K, Grosberg A. Striated myocyte structural integrity: automated analysis of sarcomeric z-discs. *PLoS Comput Biol* 2020;**16**:e1007676.
- Broadway-Stringer S, Jiang H, Wadmore K, Hooper C, Douglas G, Steeples V, Azad AJ, Singer E, Reyat JS, Galatik F, Ehler E, Bennett P, Kalisch-Smith JJ, Sparrow DB, Davies B, Djinić-Carugo K, Gautel M, Watkins H, Gehrmlich K. Insights into the role of a cardiomyopathy-causing genetic variant in ACTN2. *Cells* 2023;**12**:721.
- Livak KJ, Schmittgen TD. Analysis of relative gene expression data using real-time quantitative PCR and the 2(-Delta Delta C(T)) method. *Methods* 2001;**25**:402–408.
- Mookerjee SA, Gerencser AA, Nicholls DG, Brand MD. Quantifying intracellular rates of glycolytic and oxidative ATP production and consumption using extracellular flux measurements. *J Biol Chem* 2017;**292**:7189–7207.
- Mookerjee SA, Nicholls DG, Brand MD. Determining maximum glycolytic capacity using extracellular flux measurements. *PLoS One* 2016;**11**:e0152016.
- Mookerjee SA, Gonçalves RLS, Gerencser AA, Nicholls DG, Brand MD. The contributions of respiration and glycolysis to extracellular acid production. *Biochim Biophys Acta* 2015;**1847**:171–181.
- Litvinukova M, Talavera-Lopez C, Maatz H, Reichart D, Worth CL, Lindberg EL, Kanda M, Polanski K, Heinig M, Lee M, Nadelmann ER, Roberts K, Tuck L, Fasouli ES, DeLaughter DM, McDonough B, Wakimoto H, Gorham JM, Samari S, Mahbubani KT, Saeb-Parsy K, Patone G, Boyle JJ, Zhang H, Zhang H, Viveiros A, Oudit GY, Bayraktar OA, Seidman JG, Seidman CE, Nosedá M, Hubner N, Teichmann SA. Cells of the adult human heart. *Nature* 2020;**588**:466–472.
- Wolock SL, Lopez R, Klein AM. Scrublet: computational identification of cell doublets in single-cell transcriptomic data. *Cell Syst* 2019;**8**:281–291.e289.
- Traag VA, Waltman L, van Eck NJ. From Louvain to Leiden: guaranteeing well-connected communities. *Sci Rep* 2019;**9**:5233.
- Gayoso A, Lopez R, Xing G, Boyeau P, Valiollah Pour Amiri V, Hong J, Wu K, Jayasuriya M, Mehlman E, Langevin M, Liu Y, Samaran J, Misrahi G, Nazaret A, Clivio O, Xu C, Ashuach T, Gabitto M, Lotfollahi M, Svensson V, da Veiga Beltrame E, Kleshchevnikov V, Talavera-Lopez C, Pachter L, Theis FJ, Streets A, Jordan MI, Regier J, Yosef N. A Python library for probabilistic analysis of single-cell omics data. *Nat Biotechnol* 2022;**40**:163–166.
- Mohr ME, Li S, Trouten AM, Stairley RA, Roddy PL, Liu C, Zhang M, Sucov HM, Tao G. Cardiomyocyte-fibroblast interaction regulates ferroptosis and fibrosis after myocardial injury. *iScience* 2024;**27**:109219.
- O'Shea C, Holmes AP, Yu TY, Winter J, Wells SP, Correia J, Boukens BJ, De Groot JR, Chu GS, Li X, Ng GA, Kirchhof P, Fabritz L, Rajpoot K, Pavlovic D. ElectroMap: high-throughput open-source software for analysis and mapping of cardiac electrophysiology. *Sci Rep* 2019;**9**:1389.
- Kim D, Paggi JM, Park C, Bennett C, Salzberg SL. Graph-based genome alignment and genotyping with HISAT2 and HISAT-genotype. *Nat Biotechnol* 2019;**37**:907–915.
- Li H, Handsaker B, Wysoker A, Fennell T, Ruan J, Homer N, Marth G, Abecasis G, Durbin R; 1000 Genome Project Data Processing Subgroup. The sequence alignment/map format and SAMtools. *Bioinformatics* 2009;**25**:2078–2079.
- Zeemering S, Isaacs A, Winters J, Maesen B, Bidar E, Dimopoulou C, Guasch E, Batlle M, Haase D, Hatem SN, Kara M, Kaab S, Mont L, Sinner MF, Wakili R, Maessen J, Crijns H, Fabritz L, Kirchhof P, Stoll M, Schotten U. Atrial fibrillation in the presence and absence of heart failure enhances expression of genes involved in cardiomyocyte structure, conduction properties, fibrosis, inflammation, and endothelial dysfunction. *Heart Rhythm* 2022;**19**:2115–2124.
- Nadadur RD, Broman MT, Boukens B, Mazurek SR, Yang X, van den Boogaard M, Bekeny J, Gadek M, Ward T, Zhang M, Qiao Y, Martin JF, Seidman CE, Seidman J, Christoffels V, Efimov IR, McNally EM, Weber CR, Moskowitz IP. Pitx2 modulates a tbx5-dependent gene regulatory network to maintain atrial rhythm. *Sci Transl Med* 2016;**8**:354ra115.
- Monmersteeg MT, Brown NA, Prall OW, de Gier-de Vries C, Harvey RP, Moorman AF, Christoffels VM. Pitx2c and Nkx2-5 are required for the formation and identity of the pulmonary myocardium. *Circ Res* 2007;**101**:902–909.
- Campione M, Ros MA, Icardo JM, Piedra E, Christoffels VM, Schweickert A, Blum M, Franco D, Moorman AF. Pitx2 expression defines a left cardiac lineage of cells: evidence for atrial and ventricular molecular isomerism in the iviv mice. *Dev Biol* 2001;**231**:252–264.
- Senyo SE, Steinhauser ML, Pizzimenti CL, Yang VK, Cai L, Wang M, Wu TD, Guerquin-Kern JL, Lechene CP, Lee RT. Mammalian heart renewal by pre-existing cardiomyocytes. *Nature* 2013;**493**:433–436.
- Monmersteeg MT, Hoogaars WM, Prall OW, de Gier-de Vries C, Wiese C, Clout DE, Papaioannou VE, Brown NA, Harvey RP, Moorman AF, Christoffels VM. Molecular pathway for the localized formation of the sinoatrial node. *Circ Res* 2007;**100**:354–362.
- Venteclef N, Guglielmi V, Balse E, Gaborit B, Cotillard A, Atassi F, Amour J, Leprince P, Dourou A, Clement K, Hatem SN. Human epicardial adipose tissue induces fibrosis of the atrial myocardium through the secretion of adipokines. *Eur Heart J* 2015;**36**:795–805.
- Suffee N, Baptista E, Piquereau J, Ponnaiah M, Doisne N, Ichou F, Lhomme M, Pichard C, Galand V, Mougnot N, Dilanian G, Lucats L, Balse E, Mericskay M, Le Goff W, Hatem SN. Impacts of a high-fat diet on the metabolic profile and the phenotype of atrial myocardium in mice. *Cardiovasc Res* 2022;**118**:3126–3139.
- Marrouche NF, Wilber D, Hindricks G, Jais P, Akoum N, Marchlinski F, Kholmovski E, Burgon N, Hu N, Mont L, Deneke T, Duytschaever M, Neumann T, Mansour M, Mahnkopf C, Herweg B, Daoud E, Wissner E, Bannmann P, Brachmann J. Association of atrial tissue fibrosis identified by delayed enhancement MRI and atrial fibrillation catheter ablation: the DECAAF study. *JAMA* 2014;**311**:498–506.



49. Li J, Qi X, Ramos KS, Lanter E, Keijer J, de Groot N, Brundel B, Zhang D. Disruption of sarcoplasmic Reticulum-mitochondrial contacts underlies Contractile dysfunction in experimental and human atrial fibrillation: a key role of mitofusin 2. *J Am Heart Assoc* 2022;**11**: e024478.
50. Chang CN, Singh AJ, Gross MK, Kioussi C. Requirement of Pitx2 for skeletal muscle homeostasis. *Dev Biol* 2019;**445**:90–102.
51. Tao G, Kahr PC, Morikawa Y, Zhang M, Rahmani M, Heallen TR, Li L, Sun Z, Olson EN, Amendt BA, Martin JF. Pitx2 promotes heart repair by activating the antioxidant response after cardiac injury. *Nature* 2016;**534**:119–123.
52. Li L, Tao G, Hill MC, Zhang M, Morikawa Y, Martin JF. Pitx2 maintains mitochondrial function during regeneration to prevent myocardial fat deposition. *Development* 2018;**145**: dev168609.
53. Porter C, Hurren NM, Cotter MV, Bhattarai N, Reidy PT, Dillon EL, Durham WJ, Tuvdendorj D, Sheffield-Moore M, Volpi E, Sidossis LS, Rasmussen BB, Borsheim E. Mitochondrial respiratory capacity and coupling control decline with age in human skeletal muscle. *Am J Physiol Endocrinol Metab* 2015;**309**:E224–E232.
54. Rizvi F, Preston CC, Emelyanova L, Yousufuddin M, Viqar M, Dakwar O, Ross GR, Faustino RS, Holmuhamedov EL, Jahangir A. Effects of aging on cardiac oxidative stress and transcriptional changes in pathways of reactive oxygen Species generation and clearance. *J Am Heart Assoc* 2021;**10**:e019948.
55. Zelniker TA, Bonaca MP, Furtado RHM, Mosenzon O, Kuder JF, Murphy SA, Bhatt DL, Leiter LA, McGuire DK, Wilding JPH, Budaj A, Kiss RG, Padilla F, Gause-Nilsson I, Langkilde AM, Raz I, Sabatine MS, Wiviott SD. Effect of dapagliflozin on atrial fibrillation in patients with type 2 diabetes Mellitus: insights from the DECLARE-TIMI 58 trial. *Circulation* 2020;**141**: 1227–1234.
56. Kolijn D, Pabel S, Tian Y, Lodi M, Herwig M, Carrizzo A, Zhazykbayeva S, Kovacs A, Fulop GA, Falcao-Pires I, Reusch PH, Linthout SV, Papp Z, van Heerebeek L, Vecchione C, Maier LS, Ciccarelli M, Tschope C, Mugge A, Bagi Z, Sossalla S, Hamdani N. Empagliflozin improves endothelial and cardiomyocyte function in human heart failure with preserved ejection fraction via reduced pro-inflammatory-oxidative pathways and protein kinase Galpha oxidation. *Cardiovasc Res* 2021;**117**:495–507.
57. Zhang D, Hu X, Li J, Liu J, Baks-Te Bulte L, Wiersma M, Malik NU, van Marion DMS, Tolouee M, Hoogstra-Berends F, Lanter EAH, van Roon AM, de Vries AAF, Pijnappels DA, de Groot NMS, Henning RH, Brundel B. DNA damage-induced PARP1 activation confers cardiomyocyte dysfunction through NAD(+) depletion in experimental atrial fibrillation. *Nat Commun* 2019;**10**:1307.
58. Li Q, Su D, O'Rourke B, Pogwizd SM, Zhou L. Mitochondria-derived ROS bursts disturb ca(2)(+) cycling and induce abnormal automaticity in Guinea pig cardiomyocytes: a theoretical study. *Am J Physiol Heart Circ Physiol* 2015;**308**:H623–H636.
59. Hegyi B, Polonen RP, Hellgren KT, Ko CY, Ginsburg KS, Bossuyt J, Mercola M, Bers DM. Cardiomyocyte Na(+) and Ca(2+) mishandling drives vicious cycle involving CaMKII, ROS, and ryanodine receptors. *Basic Res Cardiol* 2021;**116**:58.
60. Tow BD, Deb A, Neupane S, Patel SM, Reed M, Loper AB, Eliseev RA, Knollmann BC, Gyorko S, Liu B. SR-Mitochondria crosstalk shapes Ca signalling to impact pathophenotype in disease models marked by dysregulated intracellular Ca release. *Cardiovasc Res* 2022;**118**: 2819–2832.
61. Kim K, Blackwell DJ, Yuen SL, Thorpe MP, Johnston JN, Cornea RL, Knollmann BC. The selective RyR2 inhibitor ent-verticilide suppresses atrial fibrillation susceptibility caused by Pitx2 deficiency. *J Mol Cell Cardiol* 2023;**180**:1–9.
62. Yang R, Ernst P, Song J, Liu XM, Huke S, Wang S, Zhang JJ, Zhou L. Mitochondrial-Mediated oxidative Ca(2+)/calmodulin-dependent kinase II activation induces early afterdepolarizations in Guinea pig cardiomyocytes: an in silico study. *J Am Heart Assoc* 2018;**7**: e008939.
63. Alvarez-Franco A, Rouco R, Ramirez RJ, Guerrero-Serna G, Tiana M, Cogliati S, Kaur K, Saeed M, Magni R, Enriquez JA, Sanchez-Cabo F, Jalife J, Manzanares M. Transcriptome and proteome mapping in the sheep atria reveal molecular features of atrial fibrillation progression. *Cardiovasc Res* 2021;**117**:1760–1775.
64. Assum I, Krause J, Scheinhardt MO, Muller C, Hammer E, Borschel CS, Volker U, Conradi L, Geelhoed B, Zeller T, Schnabel RB, Heinig M. Tissue-specific multi-omics analysis of atrial fibrillation. *Nat Commun* 2022;**13**:441.
65. Li D, Liu Y, Hidru TH, Yang X, Wang Y, Chen C, Li KHC, Tang Y, Wei Y, Tse G, Xia Y. Protective effects of sodium-glucose transporter 2 inhibitors on atrial fibrillation and atrial flutter: a systematic review and meta-analysis of randomized placebo-controlled trials. *Front Endocrinol (Lausanne)* 2021;**12**:619586.
66. Maroli G, Braun T. The long and winding road of cardiomyocyte maturation. *Cardiovasc Res* 2021;**117**:712–726.
67. Campostrini G, Windt LM, van Meer BJ, Bellin M, Mummery CL. Cardiac tissues from stem cells: new routes to maturation and cardiac regeneration. *Circ Res* 2021;**128**:775–801.